

AD-A210 306

OFFICE OF NAVAL RESEARCH

Contract N00014-86-K-0556

Technical Report No. 90

Solvent Dynamical Effects in Electron Transfer:

Evaluation of Electronic Matrix Coupling Elements for  
Metallocene Self-Exchange Reactions

by

G. E. McManis, R. M. Nielson, A. Gochev, and M. J. Weaver

Prepared for Publication

in the

Journal of the American Chemical Society

Purdue University

Department of Chemistry

West Lafayette, Indiana 47907

July 1, 1989

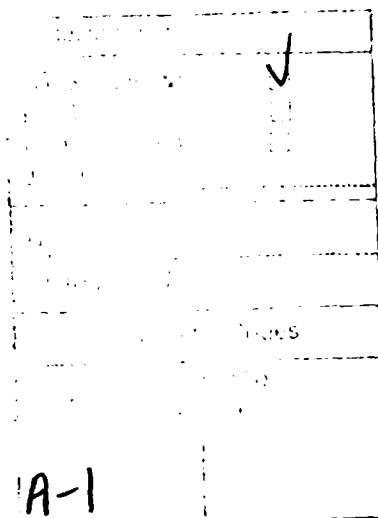
Reproduction in whole, or in part, is permitted for any purpose of the United States Government.

\* This document has been approved for public release and sale: its distribution is unlimited.

# REPORT DOCUMENTATION PAGE

|   |       |   |   |                        |
|---|-------|---|---|------------------------|
| a REPORT SECURITY CLASSIFICATION<br>Unclassified  |       |   | 1b RESTRICTIVE MARKINGS   |                        |
| a SECURITY CLASSIFICATION AUTHORITY   |       |   | 3 DISTRIBUTION/AVAILABILITY OF REPORT<br>Approved for public release and sale; its distribution is unlimited.   |                        |
| b DECLASSIFICATION/DOWNGRADING SCHEDULE   |       |   |   |                        |
| PERFORMING ORGANIZATION REPORT NUMBER(S)<br>Technical Report No. 90   |       |   | 5 MONITORING ORGANIZATION REPORT NUMBER(S)  |                        |
| a NAME OF PERFORMING ORGANIZATION<br>Purdue University<br>Department of Chemistry   |       | 6b OFFICE SYMBOL<br>(if applicable)         | 7a NAME OF MONITORING ORGANIZATION<br>Division of Sponsored Programs<br>Purdue Research Foundation  |                        |
| c ADDRESS (City, State, and ZIP Code)<br>Purdue University<br>Department of Chemistry<br>West Lafayette, Indiana 47907  |       |   | 7b ADDRESS (City, State, and ZIP Code)<br>Purdue University<br>West Lafayette, Indiana 47907  |                        |
| a NAME OF FUNDING/SPONSORING ORGANIZATION<br>Office of Naval Research   |       | 8b OFFICE SYMBOL<br>(if applicable)         | 9. PROCUREMENT INSTRUMENT IDENTIFICATION NUMBER<br>Contract No. N00014-86-K-0556  |                        |
| c ADDRESS (City, State, and ZIP Code)<br>800 N. Quincy Street<br>Arlington, VA 22217  |       |   | 10 SOURCE OF FUNDING NUMBERS  |                        |
|   |       |   | PROGRAM ELEMENT NO  | PROJECT NO             |
|   |       |   | TASK NO   | WORK UNIT ACCESSION NO |
| 1 TITLE (Include Security Classification)<br>Solvent Dynamical Effects in Electron Transfer: Evaluation of Electronic Matrix Coupling Elements for Metallocene Self-Exchange Reactions  |       |   |   |                        |
| 2 PERSONAL AUTHOR(S)<br>G. E. McManis, R. M. Nielson, A. Gochev, and M. J. Weaver   |       |   |   |                        |
| 3a TYPE OF REPORT<br>Technical  |       | 13b TIME COVERED<br>FROM 10/1/87 TO 6/30/89 | 14. DATE OF REPORT (Year, Month, Day)<br>July 1, 1989   |                        |
| 15 PAGE COUNT   |       |   |   |                        |
| 6 SUPPLEMENTARY NOTATION<br>sub ex 1/tau sub L  |       |   |   |                        |
| 7. COSATI CODES   |       |   | 18 SUBJECT TERMS (Continue on reverse if necessary and identify by block number)  |                        |
| FIELD   | GROUP | SUB-GROUP                                   | metallocene redox couples, solvent dynamics, electronic matrix coupling element, nuclear frequency factor, longitudinal solvent relaxation time tau sub L |                        |
|   |       |   |   |                        |
| 9. ABSTRACT (Continue on reverse if necessary and identify by block number)   |       |   |   |                        |
| <p>The functional dependence of the rate constants for self exchange, <math>k_{ex}</math>, for a series of metallocene redox couples to solvent-induced variations in the nuclear frequency factor, <math>\nu_n</math>, engendered by alterations in the longitudinal solvent relaxation time, <math>\tau_L</math>, are utilized to deduce values of the electronic matrix coupling element, <math>H_{12}</math>, for electron exchange. The analysis exploits the sensitivity of the <math>k_{ex} - \tau_L^{-1}</math> dependence to the degree of reaction adiabaticity and hence <math>H_{12}</math> for a given electron-exchange reaction. Six metallocene couples are examined: <math>Cp_2Co^{+/0}</math>, <math>Cp_2Fe^{+/0}</math> (<math>Cp</math> = cyclopentadienyl) and the decamethyl derivatives <math>Cp_2Co^{+/0}</math> and <math>Cp_2Fe^{+/0}</math> scrutinized previously (refs. 5a,b), additional solvent-dependent <math>k_{ex}</math> values for carboxymethyl(cobaltocenium-cobaltocene) [<math>Cp_2Co^{+/0}</math>, e = "ester"] and hydroxymethyl(ferrocenium-ferrocene) [<math>HMFC^{+/0}</math>]. Kinetic data are examined in 15 solvents, including 11 "Debye" solvents for which it is anticipated that <math>\nu_n \propto \tau_L^{-1}</math>. Corrections to <math>k_{ex}</math> for the solvent-dependent variations in the barrier height were obtained by corresponding measurements of the optical electron-transfer energies for the related binuclear complex biferrocenyl-</p> <p>(continued on back)</p> |       |   |   |                        |
| 0 DISTRIBUTION/AVAILABILITY OF ABSTRACT<br><input checked="" type="checkbox"/> UNCLASSIFIED/UNLIMITED <input checked="" type="checkbox"/> SAME AS RPT <input type="checkbox"/> DTIC USERS   |       |   | 21 ABSTRACT SECURITY CLASSIFICATION   |                        |
| 2a NAME OF RESPONSIBLE INDIVIDUAL   |       |   | 22b TELEPHONE (Include Area Code)   | 22c OFFICE SYMBOL      |

Cp = 2 is representative of



19. (cont.)

acetylene, yielding "barrier-corrected" rate constants,  $k'_{ex}$ . The  $k'_{ex} - \tau_L^{-1}$  dependencies, as well as the  $k_{ex}$  values in a given solvent, are markedly dependent on the redox couple. The  $\log k_{ex} - \log \tau_L^{-1}$  plots for the most facile couple,  $Cp_2Co^{+/0}$ , exhibit slopes approaching unity for smaller  $\tau_L^{-1}$  values. The less facile couples yield smaller slopes, diminishing in the same sequence that  $k'_{ex}$  decreases in a given solvent:  $Cp_2Co^{+/0} > Cp_2Co^{+/0} > Cp_2Co^{+/0} \gtrsim Cp_2Fe^{+/0} > Cp_2Fe^{+/0} \gtrsim HMFc^{+/0}$ . These findings are consistent with  $H_{12}$  decreasing in the same order. Comparison of such rate-solvent friction dependencies with corresponding plots calculated using a combined solvent friction-electron tunneling model yield the following approximate values of the matrix coupling element for reactant "closest approach",  $H_{12}^0$  (kcal mol<sup>-1</sup>):  $Cp_2Co^{+/0}$ , 1.0;  $Cp_2Co^{+/0}$ , 0.5-1.0;  $Cp_2Co^{+/0}$ , 0.5;  $Cp_2Fe^{+/0}$ , 0.2;  $Cp_2Fe^{+/0}$ , 0.1;  $HMFc^{+/0}$ , 0.075. Reasonable concordance is seen with recent theoretical estimates of  $H_{12}^0$  for  $Cp_2Co^{+/0}$  and  $Cp_2Fe^{+/0}$ . The relationship between  $H_{12}^0$  and metallocene electronic structure is briefly discussed. The analysis also enables effective solvent relaxation times for adiabatic barrier crossing in non-Debye media, including primary alcohols, to be extracted.

**Solvent Dynamical Effects in Electron Transfer:  
Evaluation of Electronic Matrix Coupling Elements  
for Metallocene Self-Exchange Reactions**

**George E. McManis, Roger M. Nielson, Alexander Gochev,  
and Michael J. Weaver\***

**Department of Chemistry, Purdue University  
West Lafayette, Indiana 47907**

**Running Title: Evaluation of Electronic Coupling Matrix Elements**

**J. Am. Chem. Soc.**

**In press, March 1989**

## ABSTRACT

The functional dependence of the rate constants for self exchange,  $k_{ex}$ , for a series of metallocene redox couples to solvent-induced variations in the nuclear frequency factor,  $\nu_n$ , engendered by alterations in the longitudinal solvent relaxation time,  $\tau_L$ , are utilized to deduce values of the electronic matrix coupling element,  $H_{12}$ , for electron exchange. The analysis exploits the sensitivity of the  $k_{ex} - \tau_L^{-1}$  dependence to the degree of reaction adiabaticity and hence  $H_{12}$  for a given electron-exchange reaction. Six metallocene couples are examined:  $Cp_2Co^{+/0}$ ,  $Cp_2Fe^{+/0}$  (Cp = cyclopentadienyl), and the decamethyl derivatives  $Cp_2^*Co^{+/0}$  and  $Cp_2^*Fe^{+/0}$  scrutinized previously (refs. 5a,b), additional solvent-dependent  $k_{ex}$  values for carboxymethyl(cobaltocenium-cobaltocene) [ $Cp_2^*Co^{+/0}$ , e = "ester"] and hydroxymethyl(ferrocenium-ferrocene) [HMFc $^{+/0}$ ]. Kinetic data are examined in 15 solvents, including 11 "Debye" solvents for which it is anticipated that  $\nu_n \propto \tau_L^{-1}$ . Corrections to  $k_{ex}$  for the solvent-dependent variations in the barrier height were obtained by corresponding measurements of the optical electron-transfer energies for the related binuclear complex biferrocenylacetylene, yielding "barrier-corrected" rate constants,  $k'_{ex}$ . The  $k'_{ex} - \tau_L^{-1}$  dependencies, as well as the  $k_{ex}$  values in a given solvent, are markedly dependent on the redox couple. The  $\log k'_{ex} - \log \tau_L^{-1}$  plots for the most facile couple,  $Cp_2^*Co^{+/0}$ , exhibit slopes approaching unity for smaller  $\tau_L^{-1}$  values. The less facile couples yield smaller slopes, diminishing in the same sequence that  $k'_{ex}$  decreases in a given solvent:  $Cp_2^*Co^{+/0} > Cp_2^*Co^{+/0} > Cp_2Co^{+/0} \geq Cp_2^*Fe^{+/0} > Cp_2Fe^{+/0} \geq HMFc^{+/0}$ . These findings are consistent with  $H_{12}$  decreasing in the same order. Comparison of such rate-solvent friction dependencies with corresponding plots calculated using a combined solvent friction-electron tunneling model yield the following approximate values of the matrix coupling element for reactant "closest approach",  $H_{12}^0$  (kcal mol $^{-1}$ ):  $Cp_2^*Co^{+/0}$ , 1.0;  $Cp_2^*Co^{+/0}$ , 0.5-1.0;  $Cp_2Co^{+/0}$ , 0.5;  $Cp_2^*Fe^{+/0}$ , 0.2;  $Cp_2Fe^{+/0}$ , 0.1; HMFc $^{+/0}$ , 0.075. Reasonable concordance is seen with recent theoretical estimates of  $H_{12}^0$  for  $Cp_2Co^{+/0}$  and  $Cp_2Fe^{+/0}$ . The relationship between  $H_{12}^0$  and metallocene electronic structure is briefly discussed. The analysis also enables effective solvent relaxation times for adiabatic barrier crossing in non-Debye media, including primary alcohols, to be extracted.

A central fundamental question in electron transfer of widespread current interest concerns how the extent of overlap between the donor and acceptor redox orbitals, and its role in influencing reaction rates, depends upon the electronic properties and spatial configuration. The overlap is described by the electronic matrix coupling element,  $H_{12}$ , which determines the extent of resonance splitting of the barrier top.<sup>1,2</sup> This factor exerts a crucial influence upon electron-transfer kinetics, not only by influencing the barrier shape and height but also the degree of reaction adiabaticity (i.e., the probability that electron transfer will occur once the transition state has been formed).<sup>2</sup> Recent ab initio calculations of  $H_{12}$  for simple outer-sphere electron exchange processes illustrate the sensitivity of the coupling strength to electronic structure as well as to the spatial configuration of the reacting pair.<sup>2</sup> While experimental estimates of  $H_{12}$  for optical electron transfer within binuclear complexes can be extracted from band intensities,<sup>1a</sup> the evaluation of the matrix coupling element for thermal outer-sphere electron transfer is considerably less straightforward. In spite of the importance of the latter quantity as alluded to frequently in the literature,<sup>1-3</sup> its experimental evaluation has remained largely elusive.<sup>4</sup>

We have recently been examining in detail the solvent-dependent electron-exchange kinetics of various metallocene redox couples in homogeneous solution<sup>5</sup> as well as electrode surfaces<sup>6</sup> in order to explore the role of solvent relaxation dynamics on the barrier-crossing frequencies. Of primary concern have been redox couples of the form  $\text{Cp}_2\text{M}^{+/0}$  or  $\text{Cp}'_2\text{M}^{+/0}$ , where  $\text{M} = \text{Co}$  or  $\text{Fe}$ ,  $\text{Cp}$  = cyclopentadienyl, and  $\text{Cp}'$  = pentamethylcyclopentadienyl,<sup>5,6</sup> although other metallocene couples have also been examined.<sup>6b,d</sup> During these studies, it became apparent that the rate constants for homogeneous self

exchange,  $k_{ex}$ , in a given solvent display a marked sensitivity to the metallocene electronic structure. In particular,  $k_{ex}$  values for cobaltocenium-cobaltocene couples are substantially (up to ca 10 fold) larger than for corresponding ferrocenium-ferrocene couples: up to 100 fold enhancements in  $k_{ex}$  are observed upon methylation of the Cp rings together with substituting cobalt for iron.<sup>5a,7</sup> These rate variations, especially those resulting from metal substitution, were traced primarily to the greater extent of donor-acceptor orbital overlap for the cobalt versus iron systems anticipated from the primarily ligand- versus metal-centered character of the redox orbitals.<sup>7</sup> These differences in orbital overlap and hence  $H_{12}$  are consistent both with optical electron-transfer measurements for bicobaltocene versus biferrocene cations<sup>8</sup> and with recent ab initio calculations (vide infra).<sup>9</sup>

Generally speaking, the magnitude of  $H_{12}$  for a particular internuclear configuration (i.e., precursor complex geometry) can affect the rate constant for that geometry,  $k_{et}$  ( $s^{-1}$ ), by influencing the electronic transmission coefficient,  $\kappa_{el}$ , and additionally the free-energy barrier,  $\Delta G^*$ , as in the conventional expression<sup>1b</sup>

$$k_{et} = \kappa_{el} \nu_n \exp(-\Delta G^*/RT) \quad (1)$$

where  $\nu_n$  is the nuclear frequency factor. The last term describes the net dynamics along the nuclear reaction coordinate in the vicinity of the barrier top, which may include contributions from both collective solvent and inner-shell motion. If only a narrow range of precursor geometries contributes to the bimolecular reaction (vide infra),  $k_{et}$  can be related simply to  $k_{ex}$  by

$$k_{ex} = K_p k_{et} \quad (2)$$

where  $K_p$  is the statistical probability of forming the precursor geometry.<sup>1b,10</sup> If  $H_{12}$  is very small, the reaction will be nonadiabatic such that  $\kappa_{e1} \ll 1$  and  $k_{ex} \propto H_{12}^2$ .<sup>1b,2</sup> In the adiabatic regime where  $H_{12}$  is sufficiently large so that  $\kappa_{e1} \rightarrow 1$ , the dependence of  $k_{et}$  (and hence  $k_{ex}$ ) upon  $H_{12}$  will be milder, arising primarily from the diminution in the barrier height. Evidence from both experimental<sup>1c,3,4a</sup> and theoretical<sup>2</sup> sources suggests that bimolecular reactions, even involving small inorganic reactants, are often nonadiabatic in nature.

While estimates of  $\kappa_{e1}$  and hence  $H_{12}$  could in principle be obtained from  $k_{ex}$  measurements for a single system by using Eqs. (1) and (2), uncertainties in the required estimates of  $\Delta G^\ddagger$  and  $K_p$  make this procedure of little utility. One approach is to examine the relative  $k_{ex}$  values for a series of structurally related reactions chosen so that differences in the extent of electronic coupling provide a likely major contribution to the observed rate variations.<sup>4a,7</sup> However, due to the involved dependence of  $\kappa_{e1}$  upon  $H_{12}$  this procedure requires at least an estimate of  $k_{ex}$  when  $\kappa_{e1} \rightarrow 1$  (vide infra).

An attractive, yet virtually unexplored, possibility is to examine additionally the sensitivity of  $k_{ex}$  to variations in the nuclear frequency factor  $\nu_n$ . This is because the dependence of  $k_{ex}$  upon  $\nu_n$  will be sensitive to the degree of reaction nonadiabaticity, which in turn is influenced by the magnitude of  $\nu_n$  as well as  $H_{12}$ .<sup>11,12</sup> Thus while we expect that  $k_{ex} \propto \nu_n$  under adiabatic conditions [i.e., when  $\kappa_{e1} \sim 1$ , Eq. (1)], increasing  $\nu_n$  for a given  $H_{12}$  eventually can lead to a nonadiabatic condition whereupon  $k_{ex}$  becomes independent of  $\nu_n$ , since then  $\kappa_{e1} \propto \nu_n^{-1}$ .<sup>11</sup> The form of the  $k_{ex}$ - $\nu_n$  dependence should therefore be sensitive to, and therefore diagnostic of, the magnitude of  $H_{12}$ .<sup>11</sup> While  $\nu_n$  for processes featuring large inner-shell distortions will be determined at least partly by reactant vibrations that cannot be varied

readily, the dynamics of collective solvent motion can provide the dominant contribution to  $\nu_n$  when the inner-shell barrier is small (say  $\leq 1$  kcal mol<sup>-1</sup>).<sup>13-15</sup> Substantial (up to 20-50 fold) variations in  $\nu_n$  can readily be induced under the latter conditions by judicious alterations in the solvent medium, since in many cases  $\nu_n \propto \tau_L^{-1}$ , where  $\tau_L$  is the longitudinal solvent relaxation time.<sup>5a,6a-c,13,14</sup> This enables the dependence of  $k_{ex}$  upon  $\nu_n$  to be examined provided that the rates are corrected for the corresponding variations in  $\Delta G^{*5,6}$  (vide infra).

In the present paper, we exploit such a solvent-dependent analysis to obtain  $H_{12}$  estimates for a series of six ferrocene and cobaltocene self-exchange reactions. The  $k_{ex}$  values were obtained using the proton NMR line-broadening technique, with the required solvent dependence of  $\Delta G^*$  being extracted from optical electron-transfer energies for a related binuclear system, biferrocenylacetylene cation (cf ref. 5). Some of the data used in the present analysis has been discussed previously in a related context.<sup>5</sup> However, the acquisition of additional kinetic and optical barrier data along with our recent reevaluation of the solvent-dependent kinetics for ferrocenium-ferrocene self exchange<sup>5b</sup> enable the role of orbital overlap in electron transfer to be addressed here quantitatively for the first time. Besides the parent metallocene couples  $Cp_2Fe^{+/0}$  and  $Cp_2Co^{+/0}$ , and the decamethyl derivatives  $Cp_2^*Fe^{+/0}$  and  $Cp_2^*Co^{+/0}$ , we utilize new solvent-dependent rate data for the carboxymethyl(cobaltocenium-cobaltocene) and hydroxymethyl(ferrocenium-ferrocene) couples,  $(CpCO_2Me)_2Co^{+/0}$  and  $(Cp \cdot CpCH_2OH)Fe^{+/0}$ , respectively,<sup>5c</sup> abbreviated here as " $Cp_e^*Co^{+/0}$ " (e = ester) and " $HMFe^{+/0}$ ". These latter two systems were selected initially in view of their water solubility, enabling barrier-crossing dynamics in aqueous and nonaqueous media

to be compared.<sup>5c</sup> Together, these six reactant systems are shown to span a wide (ca tenfold) range in  $H_{12}$ , from ca 0.1 to 1.0 kcal mol<sup>-1</sup>.

## EXPERIMENTAL SECTION

Carboxymethylcobaltocenium tetrafluoroborate was synthesized by stirring the corresponding carboxylic acid derivative ( $\text{CpCOOH})_2\text{Co}\cdot\text{BF}_4$ ), prepared as in ref. 16, in methanol purged with anhydrous HCl for 24 hours. Addition of  $\text{HBF}_4$  and evaporating some solvent precipitated the desired product, which was recrystallized from hot methanol. The reduced species, carboxymethylcobaltocene, was prepared by stirring a hexane suspension of the salt with a deficiency of cobaltocene. The solution was filtered to remove  $\text{Cp}_2\text{Co}\cdot\text{BF}_4$  and the filtrate evaporated to dryness under vacuum. Hydroxymethylferrocene was synthesized from trimethylaminoferrocene (Aldrich) as described in ref. 17. The oxidized form,  $(\text{Cp}\cdot\text{CpCH}_2\text{OH})\text{Fe}\cdot\text{PF}_6$ , was prepared by shaking a hexane solution of the reduced species with an acidic aqueous solution containing a twofold excess of  $\text{FeCl}_3$  until the hexane phase became colorless. After filtering, a solution of  $\text{NH}_4\text{PF}_6$  was added to the aqueous phase to precipitate the desired product. Biferrocenylacetylene (BFA) was prepared as described in ref. 18; the acetylferrocene precursor was obtained by acetylation of ferrocene as outlined in ref. 19. For all complexes, identification and purity were confirmed by proton NMR and cyclic voltammetry.

The near-infrared spectra, so to obtain optical electron-transfer energies for biferrocenylacetylene cation ( $\text{BFA}^+$ ),<sup>20-22</sup> were measured between 800 and 2000 nm with a Cary Model 17D spectrophotometer, using 1 cm quartz cells. Typically, ca 1 mM concentrations were employed so to yield maximum absorbances of about 0.2-0.5. For most solvents,  $\text{BFA}^+$  was generated from BFA

by in-situ oxidation with one equivalent of  $\text{Fe}(\text{bpy})_3(\text{PF}_6)_3$  (bpy = 2,2'-bipyridyl). In some cases (e.g. methanol), the solid  $\text{BFA}^+\text{BF}_4^-$  salt was employed. This was isolated by oxidizing BFA in nitromethane under nitrogen with a stoichiometric quantity of  $\text{AgBF}_4$  (Aldrich). After filtering, the product was isolated by adding diethyl ether.

Most details of the NMR sample preparation measurements and line-broadening data analysis are given in refs. 5a and b. Solvents were high-purity grades from Burdick and Jackson, Aldrich, or Fluka and were purified where appropriate by using standard procedures. Deuterated solvents were employed whenever feasible. However, proteated media were also used successfully by suppressing the solvent peak(s) using homonuclear irradiation at the desired resonance frequencies, with a minimum of radio-frequency power to avoid significant dielectric heating.<sup>5a</sup> Proton NMR spectra for the  $\text{HMFc}^{+/\circ}$  and  $\text{Cp}_2^*\text{Co}^{+/\circ}$  systems were collected on Nicolet NT 200 and NT 470 instruments, respectively (operated at 200.0 and 469.5 MHz). Due to peak splitting on the Cp ring protons, the line-broadening measurements for these two couples utilized the  $-\text{CH}_2-$  and methyl substituent proton resonances, respectively. A complication for the former is that the methylene resonance appears as a doublet in the pure diamagnetic species (i.e. hexamethylferrocene) due to spin-spin coupling with the hydroxyl proton. This difficulty, however, was circumvented by collapsing the doublet to a single peak by saturating the  $-\text{OH}$  resonance during NMR data acquisition. In any case, essentially equivalent line widths were obtained irrespective of  $-\text{OH}$  peak saturation, presumably due to weak  $\text{CH}_2-\text{OH}$  coupling. A difficulty faced with  $\text{Cp}_2^*\text{Co}^{+/\circ}$  is that the contact shift for the methyl protons is relatively small even at 470 MHz field, ca 12 ppm, which combined with the relatively large  $k_{\text{ex}}$  values yields relatively

small electron-exchange line broadening. Consequently, it was advisable to correct the measured line widths for magnetic field inhomogeneity. For nonaqueous solvents, this was achieved simply by subtracting the corresponding measured linewidth for the tetramethylsilane reference signal; the correction was estimated to be 1-2 Hz in  $D_2O$ . This complication increases the uncertainties in the derived  $k_{ex}$  values for the  $Cp_2^*Co^{+/0}$  couple, but they are still probably reliable to within  $\pm 20-30\%$ . For the other systems,  $k_{ex}$  is typically reproducible to 10-20%.<sup>5</sup> Experimental NMR parameters for the additional reactions studied here are summarized in the Supplementary Material.

## RESULTS AND DISCUSSION

A summary of the  $k_{ex}$  values used in the present analysis, for six redox couples in fifteen solvents, is given in Table I. Besides the additional data gathered in the present work, this summary contains pertinent data culled from refs. 5a-c (see footnote to Table I for specific details). For convenience, the  $k_{ex}$  values in Table I all refer to a uniformly low ionic strength ( $\mu \approx 0.01-0.02$  M). This entailed adjusting the values for  $Cp_2^*Co^{+/0}$  and  $Cp_2Co^{+/0}$  given earlier in ref. 5a, since these were obtained at  $\mu \approx 0.14$ . Fortunately, this correction is small (ca 25% in  $k_{ex}$ ) since  $k_{ex}$  for these metallocene couples are insensitive to variations in ionic strength, at least when "noncoordinating" anions (such as  $PF_6^-$ ,  $BF_4^-$ ) are employed.<sup>5b</sup> Kinetic data in dichloromethane and dichloroethane, reported in ref. 5a, are not included here. This is partly in view of our subsequent observation of deviations from second-order kinetics in these solvents, probably associated with complications from ion pairing. Large ion-pairing effects upon the reaction

energetics in such weakly polar media are also evident in optical electron-transfer data.<sup>21a</sup> The  $k_{ex}$  values for  $Cp_2Fe^{+/0}$ , taken in part from ref. 5b, differ substantially (up to ca 10 fold) from those reported by Wahl et al<sup>36</sup> which were utilized in our earlier solvent dynamical analyses.<sup>5a,6b</sup> The origins of the systematic solvent-dependent errors in these older data are discussed in ref. 5b. Experimental difficulties, such as reactant solubility and decomposition, along with solvent interferences and signal-to-noise constraints in the NMR line-broadening measurements, precluded the evaluation of  $k_{ex}$  for a number of redox couple/solvent combinations. For example, the ferrocene couples could not be examined in amide solvents due to decomposition. Nevertheless, sufficient kinetic, along with optical electron transfer (vide infra), data have now been assembled to enable a relatively detailed dynamical analysis to be undertaken.

Of the fifteen solvents in Table I, the first eleven are considered to approximate "Debye" dynamical behavior in that the dielectric loss spectra can be described in terms of a single relaxation time,  $\tau_D$ .<sup>37</sup> In this case, the adiabatic barrier-crossing frequency  $\nu_n$  for electron-transfer reactions having little or no inner-shell barrier is anticipated to be determined by the longitudinal relaxation time,<sup>13,14</sup> given approximately by<sup>38,39</sup>

$$\tau_L = (\epsilon_\infty/\epsilon_0) \tau_D \quad (3)$$

where  $\epsilon_\infty$  and  $\epsilon_0$  are the "infinite-" and zero-frequency solvent dielectric constants, respectively. The  $\tau_L^{-1}$  values for each of these solvents are given in Table I (see footnotes and refs. 5a and 6c for data sources); the Debye solvents are listed in order of increasing  $\tau_L$ . Rate data obtained in three likely "non-Debye" solvents - propylene carbonate, methanol, and ethanol - are

also included in this compilation, along with  $\tau_L^{-1}$  estimates for the major (low-frequency) relaxation, given in parentheses. (Such non-Debye behavior is characterized by at least one higher-frequency dispersion region having dissipative characteristics.<sup>25,33-35,37</sup>) Although the connection between the dielectric loss spectra and  $\nu_n$  is considerably less straightforward for non-Debye solvents,<sup>5a,25,40</sup> these kinetic data are nevertheless of interest to the present discussion (vide infra).

As already noted, the central thrust of the present work is to examine the sensitivity of the barrier-crossing frequency to alterations in the solvent dynamics as a means of probing the orbital-overlap factor,  $H_{12}$ . Even though only relative, rather than absolute, preexponential factors for a given reaction in a suitable series of solvents are required for this analysis, the solvent-dependent  $k_{ex}$  values still need to be corrected for differences in the barrier height,  $\Delta G^*$ . The required solvent-dependent  $\Delta G^*$  estimates can be obtained in two ways. The first involves employing theoretical models, most simply the dielectric continuum treatment of Marcus.<sup>41</sup> We have used this approach in several previous discussions.<sup>5a,6a-c</sup>

An alternative, and probably more reliable, procedure utilizes experimental energies for optical electron transfer,  $E_{op}$ , within symmetrical mixed-valence compounds that are structurally similar to the thermal electron-exchange reactions of interest.<sup>5</sup> While suitable mixed-valence systems are not abundant, the biferrocenylacetylene cation ( $BFA^+$ ) constitutes an almost ideal choice for the present purposes. Besides being structurally closely similar to the reactants of interest here, the juxtaposition of the  $Cp_2Fe^+/Cp_2Fe$  partners in the binuclear complex<sup>20</sup> roughly mimics that anticipated for the precursor complex for the thermal self-exchange reactions. Most importantly,

BFA<sup>+</sup> conforms approximately to "class II" (i.e. valence-trapped) behavior,<sup>20,42</sup> enabling solvent-dependent thermal barriers,  $\Delta G_c^*$ , to be obtained simply from<sup>1a</sup>

$$\Delta G_c^* = E_{op}/4 \quad (4)$$

It should be noted that  $\Delta G_c^*$  obtained in this manner is a "cusp" barrier, i.e. in the absence of barrier-top roundedness induced by donor-acceptor orbital overlap ( $H_{12} \rightarrow 0$ ).<sup>1a,43</sup> The actual barriers,  $\Delta G^*$ , for the present thermal reactions will depend upon the internuclear configuration as well as the metallocene electronic structure (vide infra). However, at least the solvent dependence of  $\Delta G^*$  for a given reaction, as required for the present analysis, should follow approximately the corresponding variations in  $\Delta G_c^*$ .

The  $\Delta G_c^*$  estimates obtained from the experimental  $E_{op}$  values for BFA<sup>+</sup> in each solvent are also listed in Table I. Values of  $E_{op}$  for six of these solvents were reported earlier;<sup>20</sup> the present values agree uniformly within the experimental uncertainty (2-3%). Although substantial ion-pairing effects upon  $E_{op}$  have been observed for BFA<sup>+</sup>,<sup>21</sup> these effects are small or negligible at the low anion concentrations ( $\leq 5$  mM) and relatively polar media employed for the present  $E_{op}$  measurements.<sup>21b</sup> (A brief comparison between the ionic strength dependence of  $k_{ex}$  and  $E_{op}$  is provided in ref. 5b.) The  $\Delta G_c^*$  value given for D<sub>2</sub>O was estimated from  $E_{op}$  data for the biferrocene cation, as described in ref. 5c, in view of the insolubility of BFA<sup>+</sup> in this solvent. Values of  $E_{op}$  could not be obtained for five solvents of interest here (dimethylsulfoxide and the amides) due to BFA<sup>+</sup> decomposition. Estimates of  $\Delta G_c^*$  are nevertheless given in parenthesis in Table I. These were obtained by taking advantage of the approximate correlation between  $E_{op}$  and  $(\epsilon_{op}^{-1} - \epsilon_o^{-1})$ , where  $\epsilon_{op}$  is the solvent optical dielectric constant.<sup>20,22</sup> Although there are

significant deviations from the direct proportionality between  $E_{op}$  and  $(\epsilon_{op}^{-1} - \epsilon_o^{-1})$  predicted from the dielectric continuum model,<sup>22</sup> the  $E_{op}$  values estimated in this manner are likely reliable to within at least  $\pm 0.2$  kcal mol<sup>-1</sup>. (The significance of such comparisons to the issue of noncontinuum solvent effects upon  $\Delta G_c^*$  will be addressed elsewhere.<sup>22</sup>) For simplicity, these  $\Delta G_c^*$  values are utilized for each redox couple considered here. Slightly (up to 25% smaller) values are anticipated for the decamethyl derivatives in view of their larger size on the basis of the usual continuum treatment.<sup>41</sup> However, given that only the solvent dependence of  $\Delta G_c^*$  is important for the present purposes, and that the span of values in Table I is relatively small ( $< 0.9$  kcal mol<sup>-1</sup>), such corrections exert only a small or negligible influence upon the data analysis. In any case, they are of marginal validity, especially given the uncertainties in the precise precursor geometries that contribute to  $k_{ex}$  (vide infra).

#### Rate-Solvent Friction Dependencies

In our previous analyses of solvent dynamical effects for metallocene self-exchange reactions,<sup>5</sup> we obtained solvent-dependent barrier-crossing frequencies,  $\kappa_{e1}\nu_n$ , by inserting the experimental rate constants into Eqs. (1) and (2) together with the corresponding  $\Delta G^*$  values and a suitable estimate of  $K_p$ . The manner and extent of the solvent dynamical influence upon  $k_{ex}$  can then be ascertained by examining the dependence of these inferred  $\kappa_{e1}\nu_n$  values upon known dynamical parameters, most simply  $\tau_L^{-1}$ .<sup>5</sup>

A somewhat different analysis is employed here. While this simple procedure is desirable for some purposes, as noted above the present objective hinges on examining the functional sensitivity of the net barrier-crossing

dynamics to the solvent friction, as reflected in  $\tau_L^{-1}$ . A complication in employing the preequilibrium treatment [Eq. (2)] for this purpose is that the effective  $K_p$  value for a given reaction will tend to vary somewhat with the friction rather than remain constant as is assumed in this analysis.<sup>11b</sup> This is because the distribution of precursor-complex geometries, most simply the range of donor-acceptor spatial separations ( $r$ ), contributing significantly to the bimolecular reaction rate will inexorably alter as the barrier-crossing dynamics and hence degree of reaction adiabaticity changes.<sup>11b,12</sup> Strictly speaking, the bimolecular rate constant,  $k_{ex}$ , even for a pair of "ideal" spherical reactants is composed of an integral of "local" unimolecular rate constants,  $k_{et}(r)$ , expressed as<sup>44</sup>

$$k_{ex} = (4\pi N/10^3) \int_{r_0}^{\infty} r^2 k_{et}(r) g_{DA}(r) dr \quad (5)$$

where  $N$  is Avogadro's number,  $r_0$  is the donor-acceptor distance corresponding to the reactant's closest approach, and  $g_{DA}(r)$  is the radial pair distribution function. [For simplicity,  $g_{DA}(r)$  will be taken here as unity.] The radial dependence of  $k_{et}$ , and hence  $k_{ex}$ , is determined primarily by two factors: the diminution in  $H_{12}$  (and hence of  $\kappa_{e1}$ ) and the increases in  $\Delta G^*$  expected with increasing  $r$ . On the basis of Eq. (1), both of these effects lead to  $k_{et}(r)$  decreasing sharply with increasing  $r$ . In addition, in the presence of solvent friction  $\nu_n$  is anticipated to increase significantly both with decreasing  $H_{12}$  and increasing  $\Delta G^*$ , and hence with increasing  $r$ .<sup>11,25</sup> All three terms that comprise  $k_{et}$  in Eq. (1) are therefore dependent on the precursor-complex geometry and can therefore influence the  $k_{ex} - \tau_L^{-1}$  dependence in a relatively complex fashion.<sup>11b</sup>

Although this situation may seem somewhat daunting, these complications

may be circumvented in the following manner. Since the  $\Delta G_c^*$  values in Table I span the narrow range 4.55 to 5.4 kcal mol<sup>-1</sup>, the solvent dependence of  $k_{ox}$  due to variations in the barrier height may be corrected for by

$$k'_{ox} = k_{ox} \exp[(\Delta G_c^* - 5.0)/RT] \quad (6)$$

where  $R$  is the gas constant and  $k'_{ox}$  is the rate constant that would be observed in a given solvent if the cusp-limit barrier was 5.0 kcal mol<sup>-1</sup>. Since the deviations from this average  $\Delta G_c^*$  value for the present solvents are less than 0.5 kcal mol<sup>-1</sup>, the corrections to  $k_{ox}$  amount to only twofold or less. Although the inevitable uncertainties in  $\Delta G_c^*$ , perhaps as much as 20-25% (vide supra), in the actual  $\Delta G_c^*$  values may engender some error in the derived  $k'_{ox}$  values,<sup>45</sup> at least the required relative  $k'_{ox}$  values in the various solvents should be reliable to within 50% or less. The solvent dependence of  $k'_{ox}$  will therefore reflect chiefly variations in the preexponential factor caused by alterations in the solvent friction. The nature and extent of this dependence in turn should be sensitive to, and hence diagnostic of, the degree of reaction adiabaticity, and hence  $H_{12}$ , for the precursor-complex configurations that contribute most prominently to the observed reaction rates. This procedure is related closely to our previous analysis,<sup>5a</sup> involving the estimation of solvent-dependent  $\kappa_{e1}\nu_n$  values from the measured rate constants by employing the preequilibrium treatment [Eqs. (1),(2)] and correcting for the barrier height. Such  $\kappa_{e1}\nu_n$  estimates are instructive for some purposes.<sup>5</sup> However, the spatial integration embodied in Eq. (5) necessarily considers a range of precursor geometries with spatially dependent preexponential and exponential factors (vide infra). For the present purposes, therefore, it is preferable to explore the solvent-dependent

dynamical effects in terms of  $k'_{\text{ex}}$  rather than to extract  $\nu_n$  estimates from the rate data.

Plots of  $\log k'_{\text{ex}}$  versus  $\log \tau_L^{-1}$  for five metallocene couples in eleven "Debye" solvents, extracted from the  $k_{\text{ex}}$  and  $\Delta G_c^*$  values in Table I by using Eq. (6), are given in Fig. 1. The solvent numbering scheme is as listed in Table I; the three filled symbols (circles, squares, and triangles) refer to  $\text{Cp}_2'\text{Co}^{+/0}$ ,  $\text{Cp}_2^*\text{Co}^{+/0}$ , and  $\text{Cp}_2\text{Co}^{+/0}$ , respectively, whereas the two open symbols (triangles and squares) refer to  $\text{Cp}_2\text{Fe}^{+/0}$  and  $\text{HMFc}^{+/0}$ , respectively. (The points for  $\text{Cp}_2'\text{Fe}^{+/0}$  are not shown for clarity in Fig. 1 since these are uniformly close to the corresponding  $\text{Cp}_2\text{Co}^{+/0}$  points.) Comparably shaped  $\log k'_{\text{ex}}$  -  $\log \tau_L^{-1}$  plots, yet having somewhat larger shapes, are also obtained if the dielectric continuum estimates of  $\Delta G_c^*$  (as used in ref. 5a) are employed instead to estimate  $k'_{\text{ex}}$  from  $k_{\text{ex}}$ . As noted above, however, the present experimentally derived values of  $\Delta G_c^*$  are probably more reliable than such theoretical estimates.

Inspection of Fig. 1 reveals that the degree of dependence of  $\log k'_{\text{ex}}$  upon  $\log \tau_L^{-1}$  depends markedly upon the redox couple. For the most facile  $\text{Cp}_2'\text{Co}^{+/0}$  couple, the  $\log k'_{\text{ex}}$  -  $\log \tau_L^{-1}$  slope approaches unity, yet appears to decrease as the solvent friction decreases (i.e. for higher  $\tau_L^{-1}$  values). A similar  $\log k'_{\text{ex}}$  -  $\log \tau_L^{-1}$  dependence is obtained for  $\text{Cp}_2^*\text{Co}^{+/0}$ , although the data set is more restricted. The less facile  $\text{Cp}_2\text{Co}^{+/0}$  couple also displays a qualitatively similar dependence of  $\log k'_{\text{ex}}$  upon  $\log \tau_L^{-1}$ ; however, the slopes are noticeably smaller (Fig. 1). While the  $k'_{\text{ex}}$  value for  $\text{Cp}_2\text{Co}^{+/0}$  in benzonitrile (point 8) is significantly (ca twofold) larger than expected on this basis, the remaining  $\log k'_{\text{ex}}$  -  $\log \tau_L^{-1}$  correlation is satisfactory, displaying a decidedly fractional slope (ca 0.3-0.5) towards the highest  $\tau_L^{-1}$

values. The least facile ferrocene couples  $\text{Cp}_2\text{Fe}^{+/0}$  and  $\text{HMFc}^{+/0}$  exhibit no clear dependence of  $\log k'_{\text{ex}}$  upon  $\log \tau_L^{-1}$ , even though the absence of rate data for these reactions in amides restricts somewhat the range of solvents.

Consequently, therefore, an interesting spectrum of dynamical behavior is evident. This spans the range from apparently full "solvent dynamical control", where  $k'_{\text{ex}} \propto \tau_L^{-1}$ , for the most facile cobaltocene reactions in relatively high friction (small  $\tau_L^{-1}$ ) media, to largely nonadiabatic behavior ("electron-tunneling control"), reflected in the insensitivity of  $k'_{\text{ex}}$  to  $\tau_L^{-1}$  for the least facile ferrocene systems. As outlined below, the combination of such varying rate-friction dependencies for such a "homologous series" of reactions, together with the rate differences between the reactions in a given solvent, enable *absolute* estimates of  $H_{12}$  to be obtained. Uncertainties in the data analysis together with other factors limit our confidence in some quantitative details (vide infra). Nevertheless, the solid traces included in Fig. 1 represent intuitive "best fits" of the  $\log k'_{\text{ex}} - \log \tau_L^{-1}$  dependencies for each reaction. (Only one trace is drawn for the  $\text{Cp}_2\text{Fe}^{+/0}$  and  $\text{HMFc}^{+/0}$  couples in view of their closely similar kinetic behavior).

These results are displayed in a somewhat different form in Table II, which lists  $k'_{\text{ex}}$  values ratioed to the corresponding quantity in acetonitrile,  $k'_{\text{ex}}(\text{ACN})$ . (Acetonitrile was chosen as a "reference" solvent here in view of its rapid relaxation behavior together with the availability of reliable  $k_{\text{ex}}$  values for all six metallocene couples.) Given alongside these  $k'_{\text{ex}}/k'_{\text{ex}}(\text{ACN})$  values are the corresponding  $\tau_L^{-1}/\tau_L^{-1}(\text{ACN})$  ratios, which should approximate the rate ratios only if overdamped solvent dynamical control is maintained. While the  $k'_{\text{ex}}/k'_{\text{ex}}(\text{ACN})$  values for  $\text{Cp}_2\text{Co}^{+/0}$  and  $\text{Cp}_2^*\text{Co}^{+/0}$  self exchange in Debye solvents decrease uniformly in parallel with  $\tau_L^{-1}/\tau_L^{-1}(\text{ACN})$ , the rate ratios for

the other couples in a given solvent are seen to increase in the sequence  $\text{Cp}_2'\text{Co}^{+/0} \sim \text{Cp}_2^*\text{Co}^{+/0} < \text{Cp}_2\text{Co}^{+/0} \leq \text{Cp}_2'\text{Fe}^{+/0} < \text{Cp}_2\text{Fe}^{+/0} \leq \text{HMFc}^{+/0}$ , the dependence becoming more marked as  $\tau_L^{-1}/\tau_L^{-1}(\text{ACN})$  decreases (Table II). This finding is consistent with a progressive decrease in the degree of solvent dynamical control for the less facile redox couples, the dependence of  $k'_{ex}$  upon  $\tau_L^{-1}$  being almost entirely absent for  $\text{Cp}_2\text{Fe}^{+/0}$  and  $\text{HMFc}^{+/0}$  (cf ref. 5b).

Also included in Table II are corresponding data for the three non-Debye solvents propylene carbonate (PC), methanol, and ethanol, along with the strongly hydrogen-bonded liquid N-methylformamide (NMF). In accordance with previous discussions,<sup>5a,25</sup> the  $k'_{ex}$  values for  $\text{Cp}_2^*\text{Co}^{+/0}$  and  $\text{Cp}_2\text{Co}^{+/0}$  in these solvents are much larger than expected from the corresponding  $\tau_L^{-1}$  values. By comparing the  $k'_{ex}$  values with corresponding values in Debye media so to achieve the best consistency with the other  $k'_{ex}-\tau_L^{-1}$  data, "effective" inverse relaxation times,  $\tau_{eff}^{-1}$ , can be deduced in these non-Debye solvents (cf ref. 40d). This procedure yields approximate  $\tau_{eff}^{-1}$  values as follows: PC,  $2 \times 10^{12} \text{ s}^{-1}$ ; methanol,  $\geq 3 \times 10^{12} \text{ s}^{-1}$ ; ethanol,  $4 \times 10^{12} \text{ s}^{-1}$ ; NMF,  $> 3 \times 10^{12} \text{ s}^{-1}$ . These enhanced barrier-crossing frequencies are roughly consistent with some theoretical predictions.<sup>25</sup> They are also in harmony with some very recent information on real-time polar solvation dynamics extracted from subpicosecond fluorescence measurements;<sup>46a</sup> a detailed comparison between  $\tau_{eff}$  obtained from electron-transfer and time-resolved fluorescence measurements will be featured in a forthcoming article.<sup>46b</sup>

A related illustration of the variations in the degree of electron-tunneling versus solvent-dynamical control as the solvent is altered is provided in Table III, which lists ratios of  $k_{ex}$  values for each metallocene versus that for  $\text{Cp}_2'\text{Co}^{+/0}$ ,  $k_{ex}/k_{ex}(\text{Cp}_2'\text{Co})$ , in seven solvents. The advantage of

this format is that no knowledge of the solvent dependence of the free-energy barriers is required, since this should largely cancel when the rate ratios are taken. The variations in these ratios with the solvent therefore provide a monitor of the extent to which the relative barrier-crossing frequencies for the different reactions are sensitive to the solvent dynamics. To facilitate comparison, the solvents are again listed in order of decreasing  $\tau_L^{-1}$ , although data in PC are inserted in a position commensurate with the  $\tau_{off}^{-1}$  value inferred above,  $2 \times 10^{12} \text{ s}^{-1}$ . The increasing emergence of electron-tunneling control of  $k_{ex}$  as the  $\tau_L^{-1}$  value for a given redox couple is increased, or the redox couple is altered in the sequence  $\text{Cp}_2'\text{Co}^{+/0} < \text{Cp}_2^*\text{Co}^{+/0} < \text{Cp}_2\text{Co}^{+/0} < \text{Cp}_2'\text{Fe}^{+/0} < \text{Cp}_2\text{Fe}^{+/0} < \text{HMFc}^{+/0}$ , can be discerned clearly in the progressive decreases in the  $k_{ex}/k_{ex}(\text{Cp}_2'\text{Co})$  ratios observed under these conditions (i.e. up the columns and across the rows, respectively, in Table III).

#### Extraction of Electronic Coupling Matrix Elements

A relatively direct means of extracting the extent of electronic coupling for each reaction from the results in Fig. 1 involves matching them with a corresponding sequence of curves obtained using  $k'_{ex}$  values,  $k'_{ex}(\text{calc})$ , calculated from a theoretical model for a suitable sequence of  $H_{12}$  values. Figure 2 displays such a set of  $\log k'_{ex}(\text{calc}) - \log \tau_L^{-1}$  curves obtained for the same solvents as in Fig. 1. A detailed presentation of the underlying theory forms the subject of ref. 11b. (See also the Appendix below.) Briefly, the  $k'_{ex}(\text{calc})$  values in each solvent were calculated by utilizing Eq. (5) with the spatial integration performed from a distance of closest approach,  $r_0$ , of 7.6 Å (i.e. twice the metallocene radius, 3.8 Å<sup>5a</sup>). The dependence of the "local" (unimolecular) rate constant,  $k_{et}$ , upon the reactant internuclear separation,  $r$ , required in Eq. (5), was obtained as follows. The

primary input parameters are  $r_L$ ,  $H_{12}$ , and  $\Delta G^*$ . While  $r_L$  can be considered to be  $r$ -independent for the present purposes,<sup>39</sup> both  $H_{12}$  and  $\Delta G^*$  are sensitive to the reactant pair geometry.

The  $r$  dependence of the former can be taken as<sup>2</sup>

$$(H_{12})^2 = (H_{12}^0)^2 \exp[-\alpha (r - r_0)] \quad (7)$$

where  $H_{12}^0$  is the matrix coupling element for the "closest approach" geometry. The coefficient  $\alpha$  is taken here to be the typical value  $1.25 \text{ \AA}^{-1}$ .<sup>2,11b</sup> The corresponding  $r$ -dependent barrier height is obtained from<sup>11b</sup>

$$\Delta G^* = \Delta G_c^* - H_{12} \quad (8)$$

In addition to the increases in  $\Delta G^*$  with increasing  $r$  due to corresponding decreases in  $H_{12}$ ,  $\Delta G_c^*$  and hence  $\Delta G^*$  should also increase under these conditions according to<sup>11b</sup>

$$\Delta G_c^*(r) = \Delta G_c^*(r_0) [2a(a^{-1} - r^{-1})] \quad (9)$$

where  $a$  is the reactant radius and  $\Delta G_c^*(r_0)$  is the cusp barrier height when  $r = r_0$  ( $= 2a$ ). This latter quantity was set equal to the  $\Delta G_c^*$  values given for each solvent in Table I. Although the radial dependence of  $\Delta G_c^*$  in Eq. (9) has its origin in the two-sphere dielectric continuum treatment,<sup>41</sup> it is also approximately consistent with  $r$ -dependent  $E_{op}$  measurements for biferrocene cations<sup>20</sup> and related systems.<sup>1a,f</sup> Strictly speaking, Eq. (9) presumes that  $\Delta G_c^*$  arises entirely from solvent reorganization, i.e. the inner-shell (reactant vibrational distortional) barrier,  $\Delta G_{is}^*$ , is small. Although our earlier estimates for  $\Delta G_{is}^*$  for these metallocene couples<sup>6b,7</sup> are marred by a systematic error in the bond-distance estimates, it is likely that

$\Delta G_{12}^* \approx 0.5 - 1 \text{ kcal mol}^{-1}$ .<sup>47</sup> (Note that the  $E_{op}$  estimates of  $\Delta G_c^*$  necessarily contain any inner-shell contribution to the binuclear redox system.)

In essence, the calculation of  $k_{et}(r)$  and hence  $k'_{ex}(\text{calc})$  from these parameters involves evaluating the corresponding adiabatic rate constant  $k_{et}^a(r)$ , and the corresponding modifications to account for nonadiabatic barrier crossing. The latter was accomplished here by using Eq. (A1) in the Appendix; note that generally  $k_{et} \leq k_{et}^a$ . These nonadiabatic effects ( $\kappa_{el} < 1$ ) are felt increasingly for smaller  $H_{12}$  and/or larger  $\tau_L^{-1}$ . The calculation of  $k_{et}^a$  takes into account the influences of barrier-top roundedness (i.e. non-zero  $H_{12}$ ) as well as the effect of solvent friction (via  $\tau_L$ ) upon the barrier-crossing frequency  $\nu_n$ . Equation (A1) also includes the effects of solvent inertia; these yield deviations from pure "overdamped" behavior (where  $\nu_n \propto \tau_L^{-1}$ ) anticipated in low-friction media where  $\nu_n$  approaches the transition-state theory (TST) limit, whereupon  $\nu_n$  equals the solvent inertial frequency  $\omega_o/2\pi$  and  $k_{et}^a = k^{TST}$ .<sup>6b,14,25</sup> (See Appendix and ref. 11b.)

The six sets of points shown in Fig. 2, with "best fit" curves drawn through each set, correspond to the  $H_{12}^o$  values, from 0.05 to 1.0 kcal mol<sup>-1</sup>, as indicated. (The particular solvents are identified by the same numbering scheme as in Table I and Fig. 1). By and large, the calculated curves (Fig. 2) show a striking similarity to the corresponding experimental plots in Fig. 1, in that the  $\log k'_{ex}(\text{calc}) - \log \tau_L^{-1}$  slopes decrease for smaller  $H_{12}^o$  and/or larger  $\tau_L^{-1}$ , reflecting increasing reaction nonadiabaticity. Indeed, it is interesting to note that even the scatter in the calculated points in Fig. 2 for solvents having the largest  $\tau_L^{-1}$  values ( $D_2O$ , acetone, acetonitrile, and nitromethane) is mimicked reasonably well by the experimental data in Fig. 1. (This scatter arises from the onset of an inertial limit upon  $k_{ex}$

which is solvent dependent,  $\omega_0$  being largest for  $D_2O$  and smallest for acetone<sup>25</sup>).

We therefore have reasonable confidence in extracting approximate estimates of  $H_{12}^0$  for the various experimental systems by matching the shapes of the experimental and calculated  $\log k'_{ex} - \log \tau_L^{-1}$  curves, together with the vertical displacement between them. This procedure yields the following  $H_{12}^0$  estimates (kcal mol<sup>-1</sup>):  $Cp_2Co^{+/0}$ , 1.0;  $Cp_2^*Co^{+/0}$ , 0.5-1.0;  $Cp_2Co^{+/0}$ , 0.25;  $Cp_2Fe^{+/0}$ , 0.2;  $Cp_2Fe^{+/0}$ , 0.1;  $HMFC^{+/0}$ , 0.075. As a pictorial illustration of these differences, Fig. 3 shows a pair of free energy-reaction coordinate profiles, calculated as in ref. 11a, appropriate for  $\Delta G_c^* = 5$  kcal mol<sup>-1</sup> with  $H_{12} = 1.0$  (solid curve) and 0.1 kcal mol<sup>-1</sup> (dashed curve).

The above  $H_{12}^0$  estimates for the cobaltocene systems, especially  $Cp_2Co^{+/0}$ , may well be significantly smaller than the actual values given the possibility that  $\Delta G_{1s}^*$  for these couples, are slightly (ca 0.5 kcal mol<sup>-1</sup>) larger than for the ferrocene systems.<sup>47</sup> The presence of such increased  $\Delta G_{1s}^*$  not only will decrease  $k'_{ex}$  in a given solvent, but also may diminish significantly the influence of solvent friction, i.e. depress the  $\log k'_{ex} - \log \tau_L^{-1}$  dependence.<sup>15,52</sup> At least the latter complication, however, should disappear in the dynamically most rapid solvents, where  $\tau_L^{-1}$  (or  $\omega_0/2\pi$ ) approaches the vibrational frequencies, ca 6 to 9 x 10<sup>12</sup> s<sup>-1</sup>,<sup>6b</sup> characterizing the symmetric Cp-M-Cp inner-shell distortions.<sup>15</sup> If  $\Delta G_{1s}^*$  is indeed 0.5 kcal mol<sup>-1</sup> larger for  $Cp_2Co^{+/0}$  than for  $Cp_2Fe^{+/0}$ , then to correct for this difference the  $\log k'_{ex}$  values for the former couple will need to be increased by 0.35 (i.e. ca 2.5 fold in  $k'_{ex}$ ) at the largest  $\log \tau_L^{-1}$  values in Fig. 1. This would yield a  $\log k'_{ex}$  difference of 1.0 rather than ca 0.65 for these couples in, say, acetonitrile and acetone. Assuming that  $H_{12}^0 \approx 0.1$  kcal mol<sup>-1</sup> for  $Cp_2Fe^{+/0}$ , it

can be deduced from Fig. 2 that this correction yields an approximately twofold enhancement in the  $H_{12}^0$  estimate for  $Cp_2Co^{+/0}$ , from ca 0.25 to 0.5 kcal  $mol^{-1}$ .

The ca 3 fold larger  $k'_{ex}$  values for  $Cp_2'Co^{+/0}$  relative to  $Cp_2Co^{+/0}$  observed in each solvent may also be attributable in part to differences in  $\Delta G_{1s}^*$ .<sup>47</sup> This behavior is also consistent with a smaller outer-shell (solvent reorganization) barrier for the former couple that might be anticipated from its slightly larger effective radius. Alternatively,  $H_{12}^0$  for  $Cp_2'Co^{+/0}$  may be even larger than 1.0 kcal  $mol^{-1}$ . Apart from the uncertainties in extracting the solvent-dependent  $k'_{ex}$  values themselves, the estimated  $\tau_L$  values are subject to significant error.<sup>39a</sup> The assumption that the first eleven solvents in Table I exhibit Debye behavior is, of course, only an approximation, even though the most recent subpicosecond time-resolved fluorescence data yields major relaxation times that typically differ from  $\tau_L$  by twofold or less.<sup>39a</sup> [The observed positive deviations of the  $k'_{ex}$  values from the anticipated  $\log k'_{ex} - \log \tau_L^{-1}$  plots in benzonitrile, for example (Fig. 1), may be due to the influence of a higher-frequency relaxation in this solvent.] Possible solvent-specific effects upon the approach of the reacting partners, which would be reflected in non-unit  $g_{DA}(r)$  values [Eq. (5)], may also contribute significantly to the rate-solvent dependence. Generally speaking, however, consideration of these and related factors lead only to relatively minor (< 2 fold) uncertainties in the inferred  $H_{12}^0$  estimates. The relative  $H_{12}^0$  values, then, are deemed sufficiently reliable to warrant at least semiquantitative interpretation.

#### Interpretation and Implications of $H_{12}^0$ Values

The markedly (ca 2.5 - 5 fold) larger  $H_{12}^0$  values estimated for  $Cp_2Co^{+/0}$

and other cobaltocene couples compared with their ferrocene analogs can be accounted for in terms of the spatial differences in the "redox molecular orbitals", corresponding to the LUMO/HOMO pair<sup>53</sup> for the  $\text{Cp}_2\text{M}^+/\text{Cp}_2\text{M}$  reaction partners.<sup>7</sup> While theoretical studies indicate that the cobaltocene HOMO is delocalized over the Cp rings,<sup>54</sup> that for ferrocene is strongly metal centered.<sup>55</sup> Since similar considerations also apply to the LUMO for the oxidized redox forms,<sup>54a,b,55</sup> the donor-acceptor orbital overlap should be greater for the  $\text{Cp}_2\text{Co}^{+/0}$  versus the  $\text{Cp}_2\text{Fe}^{+/0}$  couples.<sup>7</sup> The relative  $H_{12}^0$  values for these reactions are in harmony with the twofold greater  $H_{12}$  estimates derived from optical electron transfer data for bicobaltocene versus biferrocene cations,<sup>8</sup> although the absolute values of the latter are much larger (3.2 and 1.7 kcal mol<sup>-1</sup>, respectively) partly as a result of direct bond formation between the redox centers.

Very recent ab initio calculations by Newton also yield markedly (ca 3-6 fold) larger  $H_{12}$  values for  $\text{Cp}_2\text{Co}^{+/0}$  than for  $\text{Cp}_2\text{Fe}^{+/0}$  self exchange.<sup>9</sup> These calculations also indicate that considerably stronger overlap is obtained for approach of the reacting pair along a common fivefold axis ("axial" geometry) than for a "side-by-side" configuration. For the former geometry,  $H_{12} = 2.5$  and 0.4 kcal mol<sup>-1</sup> for  $\text{Cp}_2\text{Co}^{+/0}$  and  $\text{Cp}_2\text{Fe}^{+/0}$ , respectively, when the Cp rings are "in contact" (3.5 Å apart); whereas in the latter configuration,  $H_{12}^0 \approx 0.04$  and 0.1 kcal mol<sup>-1</sup>, respectively. These findings foreshadow a limitation in the present analysis; the substantial anisotropy in the calculated  $H_{12}$  values suggests that the assumption of spherical symmetry embodied in Eq. (5) is, strictly speaking, inadequate. Nevertheless, the present experimental  $H_{12}^0$  estimates should represent at least weighted averages of the true values for the various "close contact" encounter pair geometries, and as such are reasonably consistent with the calculated values. It would be

of interest to perform more sophisticated kinetic analyses employing such detailed theoretical information.

Interpretation of the substantial observed variation in  $H_{12}^0$  resulting from Cp ring substitution, unlike alteration of the metal center, is limited by the lack of electronic structural information for these systems. At first sight, one might expect that  $H_{12}^0$  would correlate roughly with empirical electronic quantities such as the Hammett  $\sigma$  parameter which characterizes substituent effects in organic chemistry,<sup>58</sup> especially since they correlate well with metallocene formal potentials<sup>59,60</sup> and NMR chemical shifts.<sup>61</sup>

To this end, Table IV contains  $k_{ex}$  values in acetonitrile for the self-exchange reactions studied here, together with some additional data for four monosubstituted ferrocenes,<sup>57</sup> in comparison with corresponding formal potentials,  $E_f$ . (The entries are listed in order of increasing  $E_f$ .) As noted above, the differences in  $k_{ex}$  in this dynamically rapid solvent should be particularly sensitive to variations in  $H_{12}$ . The lack of any correlation between  $k_{ex}$  and  $E_f$  for either the cobaltocene and ferrocene couples is clearly evident, even though substantial variations in both these quantities are observed. Upon reflection, however, this finding is unsurprising since the substituent effect upon  $E_f$  arises from alterations in the energy of the redox orbital, whereas  $H_{12}$  and hence  $k_{ex}$  is responsive primarily to the spatial properties of the HOMO/LUMO pair.<sup>62</sup> Given the magnitude of such apparent substituent effects upon  $H_{12}$ , their further detailed examination would be of great interest.

As noted previously,<sup>7</sup> the sensitivity of the self-exchange kinetics to the metallocene structure contrasts with the exchange kinetics of these systems at metal electrodes. In the latter environments, uniformly facile kinetics are obtained that apparently exhibit a strong dependence upon the

solvent dynamics, indicative of essentially adiabatic behavior.<sup>5a,6b,7</sup> The likelihood that this behavior persists for ferrocenium-ferrocene couples at electrodes, even in solvents such as acetonitrile,<sup>7</sup> suggests that electrochemical exchange processes may proceed by inherently more adiabatic pathways than for related self-exchange reactions. Indeed, such a conclusion is in harmony with the prediction of recent theoretical treatments.<sup>63</sup>

Although detailed theoretical calculations of  $H_{12}^0$  have only been undertaken so far for a relatively narrow range of homogeneous-phase self-exchange reactions,<sup>2</sup> most values are substantially below both the magnitude,  $\leq 0.2$  kcal mol<sup>-1</sup>, necessary to maintain a significant degree of reaction adiabaticity in dynamically rapid solvents, such as water. At least in homogeneous solution, then, the range of outer-sphere reactions influenced importantly by solvent friction effects may well be smaller than those subject primarily to electron-tunneling control of the barrier-crossing frequency. Although the present solvent-dependent analysis is applicable only in unusually favorable circumstances, it would be of considerable interest to utilize it to explore electronic coupling factors in other types of processes, especially involving intramolecular electron transfer.

#### Acknowledgments

We are grateful to Dr. Marshall Newton for providing details of his matrix element calculations for metallocenes prior to publication. Helpful discussions with Dr. David Beretan, along with preprints of ref. 12, contributed significantly to the rate-friction analysis. The NMR instruments used in this work are supported by National Institutes of Health Grant RR01077 at Purdue University. This research program is supported by the Office of Naval Research.

### Appendix

A key element in obtaining the calculated  $k'_{ex}$  values,  $k'_{ex}(\text{calc})$ , shown in Fig. 2 involves the computation of unimolecular rate constants,  $k_{et}(r)$ , that span the full range from entirely nonadiabatic to adiabatic behavior. For this purpose, we use the following relation, derived in ref. 11b:

$$k_{et}(r) = \frac{\bar{\kappa}_{e1} k^{TST}}{1 - \bar{\kappa}_{e1} + [\bar{\kappa}_{e1} k^{TST}/k_{et}^a(r)]} \quad (A1)$$

where  $k_{et}^a(r)$  is the rate constant for adiabatic barrier crossing, and  $k^{TST}$  is the rate constant corresponding to the TST limit (i.e. in the absence of solvent friction) given by

$$k^{TST} = (\omega_0/2\pi) \exp(-\Delta G^*/RT) \quad (A2)$$

where  $\omega_0$  is the solvent inertial frequency. The electronic transmission coefficient,  $\bar{\kappa}_{e1}$ , can be related to the more familiar  $\kappa_{e1}$  in Eq. (1) by (see Appendix to ref. 11b)

$$\kappa_{e1} = \bar{\kappa}_{e1}/[\kappa_a + \bar{\kappa}_{e1}(1 - \kappa_a)] \quad (A3)$$

where the "adiabatic transmission coefficient"  $\kappa_a = k_{et}^a/k^{TST}$ .

Apart from the additional  $-\bar{\kappa}_{e1}$  term in the denominator, Eq. (A1) is similar or identical to other literature relations for interpolating between the adiabatic and nonadiabatic limits (e.g. refs. 12, 13). This term allows  $k_{et}(r)$  to reduce to the correct adiabatic TST limit, whereupon the preexponential factor equals  $\omega_0/2\pi$ .<sup>11b</sup>

The adiabatic rate constant  $k_{et}^a$  was calculated using a position (q)-dependent diffusional model, whereby the diffusion coefficient,  $D$ , describing progress along the reaction coordinate in the presence of solvent friction

within the intersection region differs from that in the potential-energy wells as a result of barrier-top roundedness (i.e.  $H_{12} > 0$ ).<sup>11b</sup> Specifically,  $k_{ot}^a$  was approximated by

$$(k_{ot}^a)^{-1} = 2 \int_0^{q^*} dq [D(q) P_{oq}(q)]^{-1} \quad (A4)$$

where the integration is performed from the reactant well to the barrier top;  $P_{oq}(q)$  is given by

$$P_{oq}(q) \approx (2\pi/\beta \omega_0^2)^{1/2} \exp[-\beta V(q)] \quad (A5)$$

where  $\beta = (k_B T)^{-1}$  ( $k_B$  is the Boltzmann constant) and  $V(q)$  describes the potential-energy surface. Appropriate expressions for  $D(q)$  in terms of  $r_L$  (i.e. for Debye solvents) and for  $V(q)$  are given in ref. 11b, along with other pertinent details. The effect of increasing  $H_{12}$  is to decrease  $k_{ot}^a$ ; typically  $k_{ot}^a$  decreases by 2-3 fold as  $H_{12}$  increases from 0 to 1 kcal mol<sup>-1</sup>, the effect depending somewhat on the extent of solvent friction. The results are numerically similar to those obtained<sup>11a</sup> by utilizing the Smoluchowski treatment of Calef and Wolynes.<sup>14</sup> (Note that the effect of solvent friction upon  $k_{ot}^a$ , as given by Eq. (A1), is contained entirely within the  $k_{ot}^a$  term.)

The  $\bar{\kappa}_{o1}$  values were calculated by using the approximate expression<sup>11b</sup>

$$\bar{\kappa}_{o1} = 4\pi^{3/2} \gamma_T / (1 + 4\pi^{3/2} \gamma_T) \quad (A6)$$

where

$$\gamma_T = |H_{12}|^2 / 4\hbar \omega_0 (\Delta G^* k_B T)^{1/2} \quad (A7)$$

For the present purposes, it is most important to note that the derived values of  $\bar{\kappa}_{o1}$ , and hence the form of the  $\log k_{ox}(\text{calc}) - \log r_L^{-1}$  curves in Fig. 2, are insensitive to the particular expression used for  $\bar{\kappa}_{o1}$ .<sup>11b</sup>

### References and Notes

1. For recent reviews, see (a) Creutz, C., *Prog. Inorg. Chem.*, 1983, 30, 1; (b) Sutin, N., *Prog. Inorg. Chem.*, 1983, 30, 441; (c) Newton, M. D.; Sutin, N., *Ann. Rev. Phys. Chem.*, 1984, 35, 437.
2. (a) Newton, M. D., *Int. J. Quant. Chem. Symp.*, 1980, 14, 363; (b) Newton, M. D., *ACS Symp. Ser.*, 1982, 198, 255; (c) Newton, M. D., *J. Phys. Chem.*, 1986, 90, 3734; (d) Newton, M. D., *J. Phys. Chem.*, 1988, 92, 3049.
3. For example, (a) Taube, H., *Adv. Chem. Ser.*, 1977, 162, 127; (b) Brunschwig, B. S.; Creutz, C.; McCartney, D. H.; Sham, T.-K.; Sutin, N., *Far. Disc. Chem. Soc.*, 1982, 74, 113; (c) Ulstrup, J., "Charge Transfer Processes in Condensed Media", *Lecture Notes in Chemistry* No. 10, Springer-Verlag, Berlin, 1979, p. 122; (d) Brocklehurst, B., *J. Phys. Chem.*, 1979, 83, 536; (e) Taube, H., in "Tunneling in Biological Systems", Chance, B.; DeVault, D. C.; Frauenfelder, H.; Marcus, R. A.; Schrieffer, J. R.; Sutin, N., Editors, Academic Press, New York, 1979, p. 173; see also other papers and discussion in this volume; (f) Haim, A., *Prog. Inorg. Chem.*, 1983, 30, 273; (g) Yee, E. L.; Weaver, M. J., *Inorg. Chem.*, 1980, 19, 1936; (h) Weaver, M. J.; Li, T. T.-T., *J. Phys. Chem.*, 1986, 90, 3823; (i) Balzani, V.; Scandola, F., *Inorg. Chem.*, 1986, 25, 4457.
4. (a) Endicott, J. F.; Ramasami, T., *J. Phys. Chem.*, 1986, 90, 3740, and articles cited therein; (b) Mayo, S. L.; Ellis, W. R., Jr.; Crutchley, R. J.; Gray, H. B., *Science*, 1986, 233, 948, and articles cited therein.
5. (a) Nielson, R. M.; McManis, G. E.; Golovin, M. N.; Weaver, M. J., *J. Phys. Chem.*, 1988, 92, 3441; (b) Nielson, R. M.; McManis, G. E.; Safford, L. K.; Weaver, M. J., *J. Phys. Chem.*, 1989, 93, 2152; (c) Nielson, R. M.; McManis, G. E.; Weaver, M. J., *J. Phys. Chem.*, submitted.
6. (a) Weaver, M. J.; Gennett, T., *Chem. Phys. Lett.*, 1985, 113, 213; (b) Gennett, T.; Milner, D. F.; Weaver, M. J., *J. Phys. Chem.*, 1985, 89, 2787; (c) McManis, G. E.; Golovin, M. N.; Weaver, M. J., *J. Phys. Chem.*, 1986, 90, 6563; (d) Nielson, R. M.; Weaver, M. J., *Organometallics*, in press.
7. Nielson, R. M.; Golovin, M. N.; McManis, G. E.; Weaver, M. J., *J. Am. Chem. Soc.*, 1988, 110, 1745.

8. McManis, G. E.; Nielson, R. M.; Weaver, M. J., *Inorg. Chem.*, 1988, 27, 1827.
9. Newton, M., personal communication.
10. Hupp, J. T.; Weaver, M. J., *J. Electroanal. Chem.*, 1983, 152, 1.
11. (a) McManis, G. E.; Mishra, A. K.; Weaver, M. J., *J. Chem. Phys.*, 1987, 86, 5550; (b) Gochev, A.; McManis, G. E.; Weaver, M. J., *J. Chem. Phys.*, submitted.
12. (a) Beretan, D. N.; Onuchic, J. N., *J. Chem. Phys.*, in press; (b) Onuchic, J. N.; Beretan, D. N., *J. Phys. Chem.*, 1988, 92, 4818.
13. Zusman, L. D., *Chem. Phys.*, 1980, 49, 295.
14. Calef, D. F.; Wolynes, P. G., *J. Phys. Chem.*, 1983, 87, 3387.
15. (a) Sumi, H.; Marcus, R. A., *J. Chem. Phys.*, 1986, 84, 4894; (b) Nadler, W.; Marcus, R. A., *J. Chem. Phys.*, 1987, 86, 3906.
16. Sheats, J. E.; Miller, W.; Kirsch, T., *J. Organomet. Chem.*, 1975, 91, 97.
17. Lindsay, J. K.; Hauser, C. R., *J. Org. Chem.*, 1957, 22, 355.
18. Rosenblum, M.; Brawn, N.; Papenmeier, J.; Applebaum, M., *J. Organomet. Chem.*, 1966, 6, 173.
19. Graham, R. J.; Lindsey, R. V.; Parshall, G. W.; Peterson, M. L.; Whitman, G. M., *J. Am. Chem. Soc.*, 1957, 79, 3416.
20. Powers, M. J.; Meyer, T. J., *J. Am. Chem. Soc.*, 1978, 100, 4393.
21. (a) Blackbourn, R. L.; Hupp, J. T., *Chem. Phys. Lett.*, 1988, 150, 399; (b) Blackbourn, R. L.; Hupp, J. T., in preparation.
22. McManis, G. E.; Gochev, A.; Nielson, R. M.; Weaver, M. J., *J. Phys. Chem.*, submitted.
23. Riddick, J. A.; Bunger, W. B., "Organic Solvents", Wiley-Interscience, New York, 1970.
24. Arnold, K. E.; Yarwood, J.; Price, A. H., *Mol. Phys.*, 1983, 48, 452.
25. McManis, G. E.; Weaver, M. J., *J. Chem. Phys.*, 1989, 90, 912.
26. Eloranta, J. K.; Kadaba, P. K., *Trans. Far. Soc.*, 1970, 66, 817.
27. Grant, E. H.; Shack, R., *Trans. Far. Soc.*, 1969, 65, 1519.

28. Nath, D.; Chandra, S., *J. Chem. Phys.*, 1969, 51, 5299.
29. Behret, H.; Schmithals, F.; Barthel, J., *Z. Phys. Chem.*, 1975, 96, 73.
30. Elie, V., *Bull. Chim. Soc. Belg.*, 1984, 93, 839.
31. (a) Poley, J. P., *App. Sci. Res. B*, 1955, 4, 337; (b) Guillaume, F.; Yarwood, J.; Price, A. H., *Mol. Phys.*, 1987, 62, 1307.
32. Gaumann, T., *Helv. Chim. Acta*, 1958, 41, 1956.
33. Cavell, E. A. S., *J. Chem. Soc. Far. Trans. II*, 1974, 70, 78.
34. (a) Saxton, J. A.; Bond, R. A.; Coats, G. T.; Dickinson, R. M., *J. Chem. Phys.*, 1962, 37, 2132; (b) Lane, J. A.; Saxton, J. A., *Proc. Roy. Soc. A*, 1952, 213, 400.
35. Barbenza, G. H., *J. Chim. Phys.*, 1968, 65, 906.
36. Yang, E. S.; Chan, M.-S.; Wahl, A. C., *J. Phys. Chem.*, 1980, 84, 3094.
37. Useful discussions are contained in: (a) Debye, P., "Polar Molecules", Dover, New York, 1945; (b) Hill, N. E.; Vaughan, W. E.; Price, A. H.; Davis, M., eds., "Dielectric Properties and Molecular Behavior", Van Nostrand Reinhold, London, 1969, Chapters 1 and 5; (c) Smyth, C. P., "Dielectric Behavior and Structure", McGraw-Hill, New York, 1955; (d) Böttcher, C. J. F.; Bordewyk, P., "Theory of Electric Polarization", Elsevier, Amsterdam, 1978; (e) For a shorter summary, see: Pottel, R., *Ber. Bunsenges. Phys. Chem.*, 1971, 75, 286.
38. For useful discussions of the relation between  $\tau_L$  and  $\tau_D$ , see: (a) Friedman, H. L., *J. Chem. Soc. Far. Trans. II*, 1983, 79, 1465; (b) Hubbard, J.; Onsager, L., *J. Chem. Phys.*, 1977, 67, 4850; (c) Van der Zwan, G.; Hynes, J. T., *J. Chem. Phys.*, 1982, 76, 2993; (d) Frolich, H., "Theory of Dielectrics", Oxford University Press, London, 1949, p. 72-3.
39. (a) The use of  $\tau_L$  in such solvent dynamical analyses is subject to some uncertainty due to the accompanying assumption of a dielectric continuum, as well as to uncertainties in the appropriate values of  $\epsilon_\infty$  to employ in Eq. (3) [see, for example, ref. 25 and the Appendix to ref. 11a]. However, the inclusion of solvent molecularity effects by using a mean spherical approximation (MSA) yields only small predicted alterations in  $\nu_n^{39b}$ ; (b) McManis, G. E.; Weaver, M. J., *J. Chem. Phys.*, 1989, 90, 1720.

40. (a) Hynes, J. T., J. Phys. Chem., 1986, 90, 3701; (b) Sparpaglion, M.; Mukamel, S., J. Chem. Phys., 1988, 88, 1465, 4300; (c) Rips, I.; Jortner, J., J. Chem. Phys., 1987, 87, 2090; (d) McManis, G. E.; Weaver, M. J., Chem. Phys. Lett., 1988, 145, 55..
41. Marcus, R. A., J. Chem. Phys., 1965, 43, 679.
42. In principle, bicobaltocene analogs of  $BFA^+$  and related ferrocene-based complexes could also be examined. However, beside the synthetic difficulties involved, on the basis of a recent comparison between the bicobaltocene and biferrocene cations<sup>8</sup> such species are liable to involve sufficiently strong donor-acceptor orbital overlap so to vitiate the applicability of Eq. (4).
43. Hush, N. S., Electrochim. Acta, 1968, 13, 1005.
44. (a) Tembe, B. L.; Friedman, H. L.; Newton, M. D., J. Chem. Phys., 1982, 76, 1490; (b) Newton, M. D.; Sutin, N., Ann. Rev. Phys. Chem., 1984, 35, 437.
45. A possible additional limitation to Eq. (6) is that  $E_{op}$  and hence  $\Delta G_c^*$  refer to a particular precursor complex geometry, whereas in actuality  $k_{ox}$  reflects an integral of reaction sites [Eq. (5)] with varying  $\Delta G^*$  [see Eqs. (8), (9)]. However, Eq. (6) is expected to be valid to a good approximation since the predominant contribution to  $k_{ox}$  should usually arise from geometries close to reactant "contact", for which at least the solvent dependence of  $\Delta G^*$  should be close to that for  $\Delta G_c^*$ .<sup>11b</sup>
46. (a) Kahlow, M. A.; Jarzeba, W.; Kang, T. J.; Barbara, P. F., J. Chem. Phys., 1989, 90, 151 and earlier papers cited therein; (b) Barbara, P. F.; Weaver, M. J., to be published.
47. The differences in metal-ring bond distance between the reduced and oxidized metallocene forms,  $\Delta a$ , given in refs. 6b and 7 were obtained largely from corresponding metal-Cp carbon bond distances,  $d_{M-C}$ , as listed in footnote h to Table I of ref. 6b (with literature sources), along with carbon-ring centroid distances,  $d_{C-rc}$ . However, these  $\Delta a$  values are ca 30-40% smaller than the true estimates due to a trigonometrical error. (We are grateful to Dr. Marshall Newton for bringing this point to our attention.) Employing the relevant  $d_{M-C}$  values in the Pythagorean theorem along with the corresponding  $d_{C-rc}$

values (1.19-1.20 Å) yields the following revised  $\Delta a$  values:  $\text{Cp}_2'\text{Co}^{+/0}$ , 0.065 Å;  $\text{Cp}_2\text{Co}^{+/0}$ , - 0.07 Å;  $\text{Cp}_2'\text{Fe}^{+/0}$ , -0.055 Å. (As before,<sup>6b,7</sup> we take  $\Delta a$  for  $\text{Cp}_2\text{Fe}^{+/0}$  to equal that for  $\text{Cp}_2'\text{Fe}^{+/0}$  in lieu of adequate bond-distance data for ferrocene.) Combined with the corresponding reduced force constants,  $f_r$ , for the M-Cp stretch for  $\text{Cp}_2\text{Co}^{+/0}$  and  $\text{Cp}_2'\text{Fe}^{+/0}$ ,  $4.0 \times 10^5$  and  $3.75 \times 10^5$  dyne  $\text{cm}^{-1}$ , respectively (footnote 15, ref. 7), we obtain  $\Delta G_{1s}^*$  values of about 1.4 and 0.8 kcal  $\text{mol}^{-1}$ . (Note that these  $f_r$  values refer to the effective force constant for each M-Cp "bond" as the Cp-M-Cp unit undergoes symmetric distortion; these values are equal to the sum of the individual M-Cp force constant and the "interaction force constant" derived from Raman and infrared frequencies.<sup>48,49</sup>) The revised  $\Delta G_{1s}^*$  values are about twice the former estimates,<sup>7</sup> but are only very approximate given the lack of more reliable bond-distance data (and the complete absence of solution-phase data) together with the simplified force-constant calculations. A somewhat smaller  $f_r$  value,  $2.3 \times 10^5$  dyne  $\text{cm}^{-1}$ , is obtained from Raman spectra for  $\text{Cp}_2'\text{Fe}^{+/0}$ <sup>50</sup> (footnote 17 of ref. 7), yielding  $\Delta G_{1s}^* \approx 0.5$  kcal  $\text{mol}^{-1}$ . Although corresponding vibrational data for  $\text{Cp}_2'\text{Co}^{+/0}$  are unavailable, a roughly similar  $\Delta G_{1s}^*$  estimate can be assumed for this couple. However, the apparently smaller effective Cp-M-Cp force constant observed upon methylation of ferrocene is perhaps questionable.<sup>51</sup>

48. For example, Hartley, D.; Ware, M. J., J. Chem. Soc. A, 1969, 138.
49. Herzberg, G., "Infrared and Raman Spectra of Polyatomic Molecules", Van Nostrand, New York, 1945, p. 187.
50. Duggan, D. M.; Hendrickson, D. N., Inorg. Chem., 1975, 14, 955.
51. Luthi, H. P.; Ammeter, J. H.; Almlöf, J.; Faegri, K., Jr., J. Chem. Phys., 1982, 72, 2002.
52. This effect arises since in the presence of a significant reactant distortional component, barrier passage can take place via vibrational relaxation from a significant distribution of solvent polarization states.<sup>15</sup> The presence of such an additional "vibrational reaction coordinate" will thereby enhance  $\nu_n$  to an extent that increases with increasing solvent friction (i.e. as the effective frequency characterizing solvent relaxation,  $\tau_L^{-1}$ , decreases). Consequently, the  $k_{ex} \propto \tau_L^{-1}$  slopes should be smaller in the presence of such vibrational

relaxation, to an extent that depends on its relative contribution to the effective barrier.

53. (a) LUMO - lowest unoccupied molecular orbital; HOMO - highest occupied molecular orbital; (b) Note that consideration of *molecular* orbitals derived from a basis set which includes the ligand as well as the metal center can account for so-called electron "superexchange" mechanisms which utilize predominantly ligand orbital overlap.<sup>2d</sup>
54. (a) Weber, J.; Goursoot, Penigault, E.; Ammeter, J. H.; Bachmann, J., J. Am. Chem. Soc., 1982, 104, 1491; (b) Famighetti, C.; Baerends, E. J., Chem. Phys., 1981, 62, 407.
55. (a) Zerner, M. C.; Loew, G. H.; Kirchner, R. F.; Mueller-Westerhoff, U. T., J. Am. Chem. Soc., 1980, 102, 589; (b) Bagus, P. S.; Wahlgren, U. I.; Almlöf, J., J. Chem. Phys., 1976, 64, 2324; (c) Rosch, N.; Johnson, K. H., Chem. Phys. Lett., 1974, 24, 179.
56. For example, Gordon, A. J.; Ford, R. A., "The Chemist's Companion", Wiley-Interscience, New York, 1972, p. 146.
57. Nielson, R. M., unpublished observations.
58. For example: (a) Hammett, L. P., "Physical Organic Chemistry", McGraw-Hill, New York, 2nd ed., 1968; (b) Ritchie, C. D.; Sager, W. F., Prog. Phys. Org. Chem., 1964, 2, 323.
59. (a) Hall, D. W.; Russell, C. D., J. Am. Chem. Soc., 1967, 89, 2316; (b) Little, W. F.; Reilley, C. N.; Johnson, J. D.; Sanders, A. P., J. Am. Chem. Soc., 1964, 86, 1382; (c) Kuwana, T.; Bublitz, D. E.; Hoh, G., J. Am. Chem. Soc., 1960, 82, 5811.
60. Sparser data for cobaltocene couples are given in: El Murr, N., Transition Met. Chem., 1981, 6, 321.
61. Butter, S. A.; Beachell, H. C., Inorg. Chem., 1966, 5, 1820.
62. A general influence of altering the overall electron density to the orbital overlap of the HOMO-LUMO pair might nevertheless be anticipated since the removal of the electron from the HOMO will cause alterations in the remaining electronic energy states. The implications of this "charge relaxation effect" upon H<sub>12</sub> are addressed in refs. 2c and d.

63. (a) Morgan, J. D.; Wolynes, P. G., J. Phys. Chem., 1987, 91, 874; (b) Zusman, L. D., Chem. Phys., 1987, 112, 53.
64. Press, W. H.; Flannery, B. P.; Tenkolsky, S. A.; Vetterling, W. T., "Numerical Recipes", Cambridge University Press, Cambridge, U.K., 1986, p. 126-130.

**TABLE I.** Summary of Rate Constants,  $k_{ex}$ , for Metallocene Self Exchange Reactions at 25°C, and Related Solvent-Dependent Data

| Solvent <sup>a</sup> | $\tau_L^{-1b}$<br>$10^{12} \text{ s}^{-1}$ | $10^{-7} k_{ex}, \text{ M}^{-1} \text{ s}^{-1} d$ |                                |                                 |                               |                                |                               |                      |
|----------------------|--|---|--------------------------------|---------------------------------|-------------------------------|--------------------------------|-------------------------------|----------------------|
|                      |  | $\Delta G_c^{*c}$                                 | $\text{Cp}_2'\text{Co}^{+/0e}$ | $\text{Cp}_2^*\text{Co}^{+/0f}$ | $\text{Cp}_2\text{Co}^{+/0g}$ | $\text{Cp}_2'\text{Fe}^{+/0h}$ | $\text{Cp}_2\text{Fe}^{+/0h}$ | $\text{HMFc}^{+/0f}$ |
| 1. Acetonitrile      | $4^{i,j}$                                  | 5.35  | 55                             | 20                              | 4.5                           | 3.5                            | 0.9                           | 0.55                 |
| 2. Propionitrile     | $-4^{j,k}$                                 | 5.15  |                                |                                 | 5.5                           | 3.1                            | 0.92                          | -0.9                 |
| 3. Acetone           | $3.5^k$                                    | 5.4   | 28                             | 12                              | 2.3                           | 2.2                            | 0.8                           | 0.72                 |
| 4. D <sub>2</sub> O  | $1.9^l$                                    | 5.2   |                                | $\approx 30$                    |                               |                                |                               | 1.4                  |
| 5. Nitromethane      | $4.5^m$                                    | 5.3   |                                | 24                              |                               | 3.7                            | 1.2                           | -1.4                 |
| 6. DMF               | $0.77^n$                                   | (5.0)   | 25                             |                                 | 3.2                           |                                |                               |                      |
| 7. DMSO              | $0.5^o$                                    | (4.9)   | 23                             |                                 | 3.0                           |                                | 0.95                          |                      |
| 8. Benzonitrile      | $0.2^p$                                    | 4.55  | 30                             | 8                               | 7.5                           | 6                              | 2.7                           | 1.8                  |
| 9. Nitrobenzene      | $0.2^p$                                    | 4.55  |                                | $\approx 4.5$                   |                               | 6                              | 3.0                           | 1.4                  |
| 10. TMU              | $0.17^q$                                   | (4.85)  |                                | 4.9                             | 1.55                          |                                |                               |                      |
| 11. HMPA             | $0.11^n$                                   | (4.95)  | 4.3                            |                                 | 0.67                          |                                |                               |                      |
| 12. PC               | $(0.4)^r$                                  | 5.25  | 35                             | 14                              | 3.6                           |                                | 1.2                           |                      |
| 13. NMF              | $0.27^n$                                   | (5.15)  |                                |                                 | 8.5                           |                                |                               |                      |
| 14. Methanol         | $(0.135)^s$                                | 5.2   |                                | -15                             | 9                             |                                | 1.8                           | 1.7                  |
| 15. Ethanol          | $(0.033)^t$                                | 5.0   |                                |                                 | 6                             |                                |                               |                      |

# Footnotes to Table I

<sup>a</sup> DMF - N,N-dimethylformamide, DMSO - dimethylsulfoxide, PC - propylene carbonate, NMF - N-methylformamide, TMU - tetramethylurea, HMPA - hexamethylphosphoramide.

<sup>b</sup> Inverse of longitudinal solvent relaxation time, obtained from Eq. (3) using values of  $\tau_D$  and  $\epsilon_\infty$  given in literature values cited, and  $\epsilon_0$  either from these sources or ref. 23. (In most cases, these values coincide with tabulations in refs. 5a and 6c. Where dielectric values not listed in refs. 5a or 6c are employed to estimate  $\tau_L$ , these are given following appropriate footnote to literature citation.)

<sup>c</sup> Free-energy barrier (in "cusp limit",  $H_{12} \rightarrow 0$ ) for self-exchange reactions in a given solvent, estimated from energy of intervalence band maximum,  $E_{op}$ , in near-infrared spectra for biferrocenylacetylene cation using Eq. 4. Value for  $D_2O$  estimated from corresponding  $E_{op}$  value for biferrocene cation (see ref. 5c). Values in parentheses were estimated as described in the text.

<sup>d</sup> Self-exchange rate constant of various cobalt and iron metallocene redox couples in solvent indicated, as obtained by proton NMR line broadening. Cp - cyclopentadienyl, Cp' - pentamethylcyclopentadienyl, Cp\* - monocarboxymethylcyclopentadienyl, HMFC - hexamethylferrocene. All values measured at (or extrapolated to) total ionic strengths  $\mu \approx 0.01-0.02$  M. (See ref. 5b for details of ionic-strength dependence of  $k_{ex}$ .) Reproducibility of  $k_{ex}$  values typically within ca 5-10%, except for  $Cp_2Co^{+/0}$  for which reproducibility was mostly within ca 20% (see text).

<sup>e</sup> Values taken from data in ref. 5a, but increased by ca 25% so to account for decrease of  $\mu$  from 0.14 to 0.02 M.

<sup>f</sup> Obtained in present study (also ref. 5c).

<sup>g</sup> As for footnote e, but  $k_{ex}$  values in propionitrile and ethanol obtained in present study.

<sup>h</sup> Obtained in present study, and from ref. 5b.

<sup>i</sup> Estimated from data in ref. 24.

<sup>j</sup> Effective  $\tau_L$  value, estimated by accounting for minor non-Debye characteristics of dielectric loss spectra, appearing as additional loss components at frequencies above  $\tau_D^{-1}$  (also see ref. 25).

<sup>k</sup> Estimated from data in ref. 26 (also see ref. 25).

<sup>l</sup> Ref. 27    <sup>m</sup> Ref. 28    <sup>n</sup> Ref. 29

<sup>o</sup> Ref. 30 ( $\tau_D = 19$  ps,  $\epsilon_\infty = 5.1$ ,  $\epsilon_0 = 46.7$ ).

<sup>p</sup> Ref. 31    <sup>q</sup> Ref. 32    <sup>r</sup> Ref. 33    <sup>s</sup> Refs. 34, 35    <sup>t</sup> Ref. 34

**TABLE II.** "Barrier-Corrected" Rate Constants for Metallocene Self Exchange in Various Solvents Relative to those in Acetonitrile,  $k'_{\text{ex}}/k'_{\text{ex}}(\text{ACN})$ , in Comparison with Corresponding Relative Solvent Relaxation Dynamics,  $\tau_L^{-1}/\tau_L^{-1}(\text{ACN})$

| Solvent <sup>a</sup> | $\tau_L^{-1}/\tau_L^{-1}(\text{ACN})^b$ | $k'_{\text{ex}}/k'_{\text{ex}}(\text{ACN})^c$ |                                |                              |                               |                              |                     |
|----------------------|---|---|--------------------------------|------------------------------|-------------------------------|------------------------------|---------------------|
|                      |   | $\text{Cp}_2'\text{Co}^{+/0}$                 | $\text{Cp}_2^*\text{Co}^{+/0}$ | $\text{Cp}_2\text{Co}^{+/0}$ | $\text{Cp}_2'\text{Fe}^{+/0}$ | $\text{Cp}_2\text{Fe}^{+/0}$ | $\text{HMFc}^{+/0}$ |
| Propionitrile        | ~ 1                                     |   |                                | 0.9                          | 0.65                          | 0.75                         | 1.2                 |
| Acetone              | 0.9                                     | 0.6   | 0.7                            | 0.6                          | 0.7                           | 1.0                          | 1.4                 |
| D <sub>2</sub> O     | 0.5                                     |   | 1.2                            |                              |                               |                              | 2                   |
| Nitromethane         | ≈ 1.1                                   |   | 1.1                            |                              | 1.0                           | 1.25                         | 2.3                 |
| DMF                  | 0.2                                     | 0.25  | 0.13                           | 0.4                          |                               |                              |                     |
| DMSO                 | 0.12                                    | 0.2   |                                | 0.3                          |                               | 0.5                          |                     |
| Benzonitrile         | 0.05                                    | 0.15  | 0.11                           | 0.4                          | 0.45                          | 0.8                          | 0.9                 |
| Nitrobenzene         | 0.05                                    |   | 0.06                           |                              | 0.45                          | 0.9                          | 0.7                 |
| TMU                  | 0.043                                   |   | 0.11                           | 0.15                         |                               |                              |                     |
| HMPA                 | 0.028                                   | 0.04  |                                | 0.075                        |                               |                              |                     |
| PC                   | (0.1)                                   | 0.55  | 0.6                            | 0.65                         |                               |                              | 1.9                 |
| NMF                  | 0.07                                    |   |                                | 1.4                          |                               |                              |                     |
| Methanol             | (0.035)                                 |   | 0.6                            | 1.6                          |                               | 1.55                         | 2.4                 |
| Ethanol              | (0.008)                                 |   |                                | 0.75                         |                               |                              |                     |

<sup>a</sup> See footnote a to Table I for explanation of abbreviations.

<sup>b</sup> Ratio of inverse longitudinal relaxation time for given solvent to that in acetonitrile. See Table I for  $\tau_L^{-1}$  values and data sources.

<sup>c</sup> Ratio of barrier-corrected rate constant,  $k'_{\text{ex}}$ , for given metallocene redox couple in various solvents to that in acetonitrile,  $k'_{\text{ex}}(\text{ACN})$ . Values of  $k'_{\text{ex}}$  obtained from experimental  $k_{\text{ex}}$  and  $\Delta G_c^*$  values (Table I) by using Eq. (6). See footnote d of Table I for explanation of metallocene abbreviations.

**TABLE III.** Ratios of Rate Constants for Metallocene Self Exchange to those for  $\text{Cp}_2'\text{Co}^{+/0}$ ,  $k_{\text{ex}}/k_{\text{ex}}(\text{Cp}_2'\text{Co})$ , in Various Solvents

| Solvent <sup>a</sup> | $\tau_L^{-1b}$<br>$10^{12}\text{s}^{-1}$ | $k_{\text{ex}}/k_{\text{ex}}(\text{Cp}_2'\text{Co})^c$ |                              |                               |                              |                     |
|----------------------|--|--|------------------------------|-------------------------------|------------------------------|---------------------|
|                      |  | $\text{Cp}_2^*\text{Co}^{+/0}$                         | $\text{Cp}_2\text{Co}^{+/0}$ | $\text{Cp}_2'\text{Fe}^{+/0}$ | $\text{Cp}_2\text{Fe}^{+/0}$ | $\text{HMFC}^{+/0}$ |
| Acetonitrile         | 4  | 0.35   | 0.08                         | 0.065                         | 0.015                        | 0.010               |
| Acetone              | 3.5                                      | 0.43   | 0.08                         | 0.08                          | 0.03                         | 0.025               |
| PC                   | (0.4)                                    | 0.4  | 0.11                         |                               |                              | 0.035               |
| DMF                  | 0.77                                     |  | 0.13                         |                               |                              |                     |
| DMSO                 | 0.5                                      |  | 0.13                         |                               |                              |                     |
| Benzonitrile         | 0.2                                      | 0.27   | 0.25                         | 0.20                          | 0.09                         | 0.06                |
| HMPA                 | 0.11                                     |  | 0.16                         |                               |                              |                     |

<sup>a</sup> See footnote a to Table I for explanation of abbreviations.

<sup>b</sup> Inverse longitudinal solvent relaxation time (as in Table I).

<sup>c</sup> Calculated from  $k_{\text{ex}}$  values in Table I.

**TABLE IV.** Comparison between Self-Exchange Rate Constants for Various Metallocene Redox Couples in Acetonitrile at 25°C and Corresponding Formal Potentials

| Redox Couple <sup>a</sup>     | $E_f^b$               | $k_{ex}^c$        |
|-------------------------------|-----------------------|-------------------|
|                               | V. vs. $Cp_2Fe^{+/0}$ | $M^{-1} s^{-1}$   |
| $Cp_2Co^{+/0}$                | -1.92                 | $5.5 \times 10^8$ |
| $Cp_2Co^{+/0}$                | -1.30                 | $4.5 \times 10^7$ |
| $Cp_2^*Co^{+/0}$              | -0.79                 | $2.0 \times 10^8$ |
| $Cp_2Fe^{+/0}$                | -0.50                 | $3.5 \times 10^7$ |
| $(Cp \cdot CpCH_2OH)Fe^{+/0}$ | -0.01                 | $5.5 \times 10^6$ |
| $Cp_2Fe^{+/0}$                | 0                     | $9 \times 10^6$   |
| $(Cp \cdot CpI)Fe^{+/0}$      | 0.15                  | $9.2 \times 10^6$ |
| $(Cp \cdot CpCOCH_3)Fe^{+/0}$ | 0.24                  | $8.0 \times 10^6$ |
| $(Cp \cdot CpCN)Fe^{+/0}$     | 0.36                  | $5.7 \times 10^6$ |

<sup>a</sup> Nomenclature partly as in Tables I-III. [Note that hydroxymethyl(ferrocenium-ferrocene) is abbreviated as  $(Cp \cdot Cp \cdot CH_2OH)Fe^{+/0}$  rather than  $HMFc^{+/0}$  for consistency with other monosubstituted ferrocenes listed here.]

<sup>b</sup> Formal potential (volts) versus ferrocenium-ferrocene in same solvent (acetonitrile) evaluated at gold or mercury electrodes in 0.1 M tetrabutylammonium hexafluorophosphate by using cyclic voltammetry.

<sup>c</sup> Rate constant for metallocene self-exchange in acetonitrile, for ionic strength  $\mu \sim 0.02$  M, taken from Table I and ref. 57. Values reproducible generally to  $\pm 10$ -20%.

## Figure Captions

### Fig. 1

Logarithmic plots of "barrier-corrected" rate constants,  $k'_{ox}$ , versus inverse of longitudinal relaxation time,  $\tau_L^{-1}$ , for five metallocene redox couples in eleven solvents.  $k'_{ox}$  values were extracted from experimental  $k_{ox}$  and  $\Delta G_c^*$  values given in Table I by using Eq. (6). See Table I for solvent numbering scheme. Key to redox couples:  $Cp_2^*Co^{+/0}$ , filled circles;  $Cp_2^*Co^{+/0}$ , filled squares;  $Cp_2Co^{+/0}$ , filled triangles;  $Cp_2Fe^{+/0}$ , open triangles;  $HMFc^{+/0}$ , open squares. Solid traces through each set of solvent-dependent  $\log k'_{ox}$  values are suggested "best fit" curves (see text).

### Fig. 2

Logarithmic plots of calculated "barrier-corrected" rate constants,  $k'_{ox}(\text{calc})$ , versus inverse of longitudinal relaxation time,  $\tau_L^{-1}$ , in same eleven solvents as for Fig. 1, for the sequence of six electronic matrix coupling elements at reactant "contact",  $H_{12}^0$ , as indicated. Values of  $k'_{ox}(\text{calc})$  obtained from corresponding calculated values,  $k_{ox}(\text{calc})$ , in each solvent by using Eq. (6) in the same manner as the experimental quantities. Values of  $k_{ox}(\text{calc})$  obtained by using spatial integration procedure [Eq. (5)] with  $r_0$  taken as 7.6 Å, and  $g_{DA}(r) = 1$ . Required values of  $k_{et}(r)$  obtained from Eq. (A1) with constituent quantities calculated as follows:  $k^{IST}$  from Eq. (A2) using "solvent inertial" frequencies,  $\omega_0$ , calculated as described in ref. 25 (see footnotes to Fig. 4 and Table II of ref. 25 for numerical values);  $k_{et}^*(r)$  from Eqs. (9)-(16) of ref. 11b;  $\bar{\kappa}_{01}$  from Eqs. (20), (20a) of ref. 11b. The  $r$ -dependent  $\Delta G^*$  values required for  $k^{IST}$  and

$k_{01}^*(r)$  were obtained from Eqs. (8) and (9) with  $\Delta G_c^*(r_0)$  as given in Table I and  $a = 3.8 \text{ \AA}$ . The  $r$ -dependent  $H_{12}$  values also required in Eq. (8), as well as for calculating  $\bar{\kappa}_{01}$ , were obtained from Eq. (7) with  $\alpha = 1.25 \text{ \AA}^{-1}$ . The double integrals required using this overall procedure (both spatially and along the reaction coordinate<sup>11b</sup>) were evaluated using a standard two dimensional quadrature technique,<sup>64</sup> executed on the Purdue University Cyber 205 supercomputer using double precision (128 bit).

### Fig. 3

Schematic free energy - reaction coordinate profiles for electron-exchange reactions having different electronic matrix coupling elements,  $H_{12}$ . Curves calculated by using Eqs. (4) and (5) of ref. 11a. For a  $5 \text{ kcal mol}^{-1}$  cusp barrier, the solid and dashed traces shown correspond to  $H_{12}$  values of  $1.0$  and  $0.1 \text{ kcal mol}^{-1}$ , respectively.

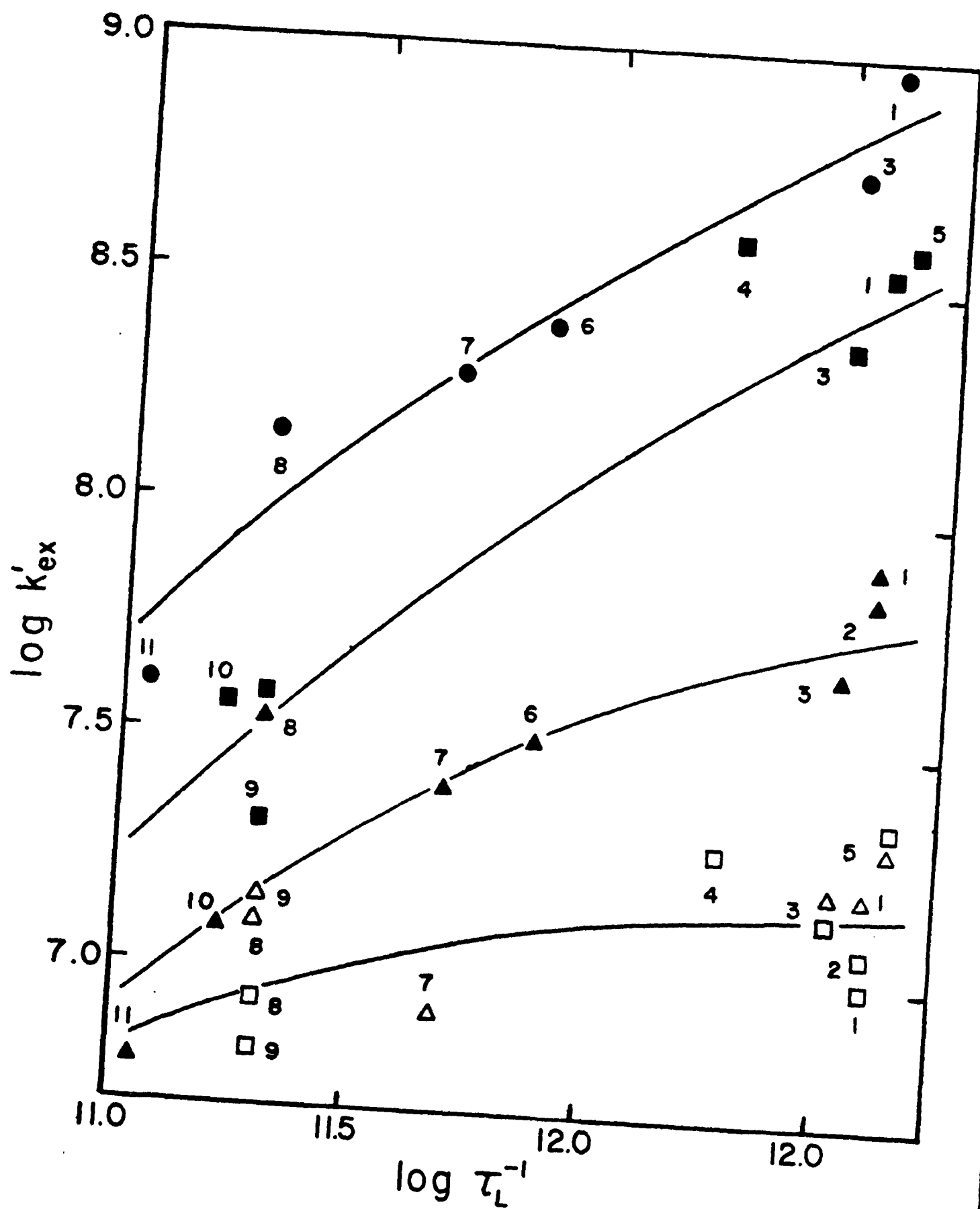


FIG 1

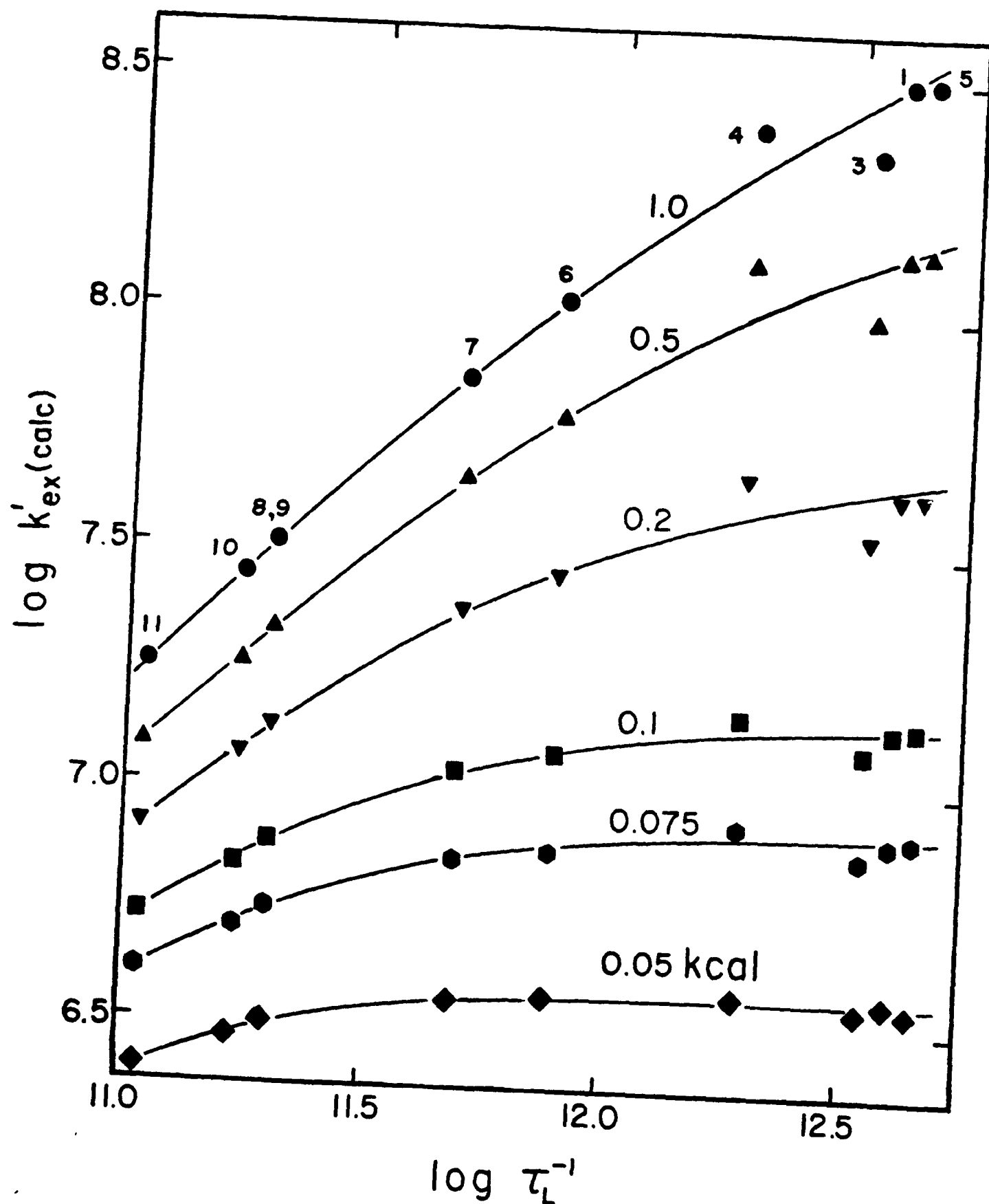


FIG 2

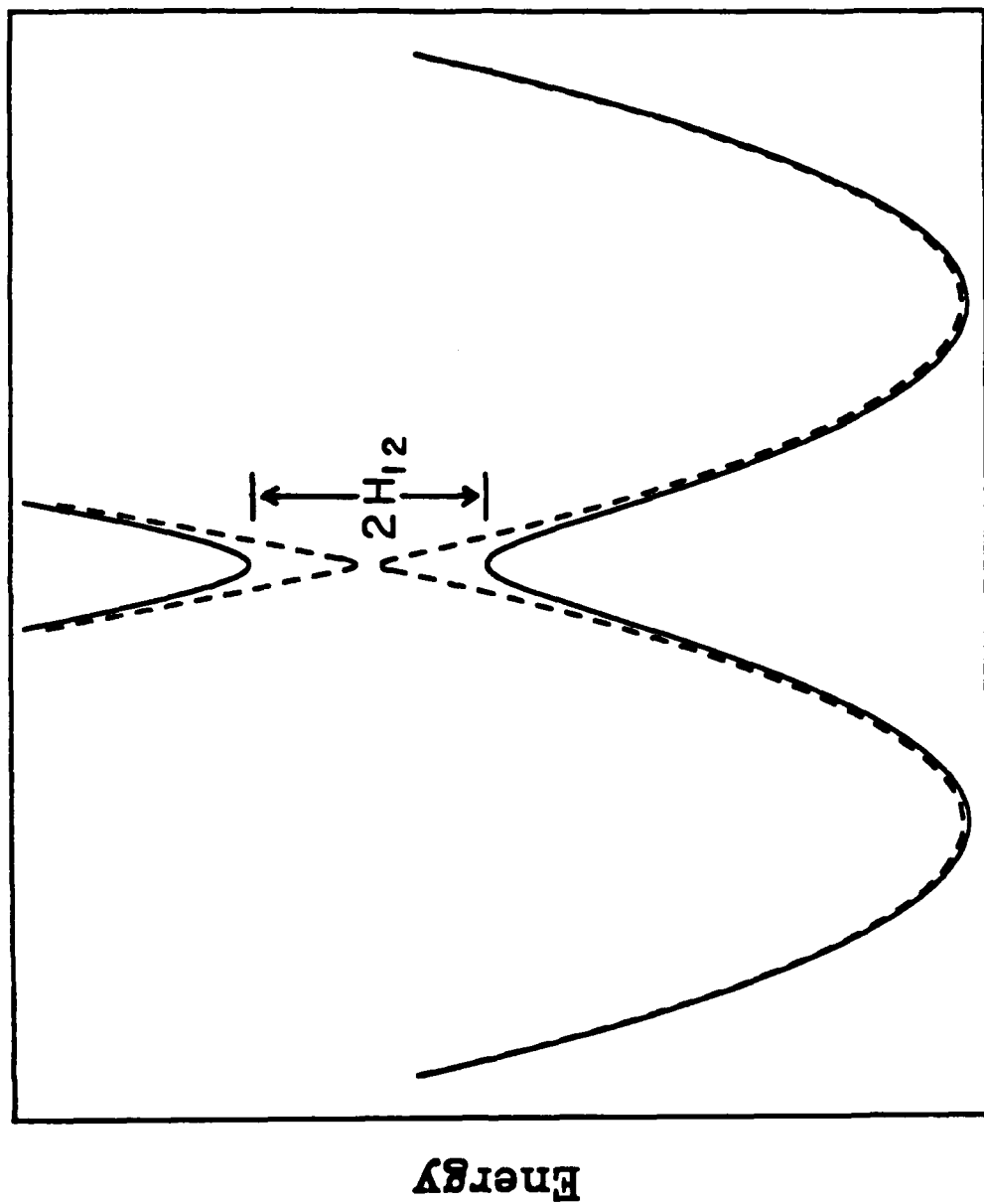


FIG 3

# SUPPLEMENTARY MATERIAL

## <sup>1</sup>H NMR Parameters and Related Data for Metallocene Self Exchange

| Solvent <sup>a</sup>   | [Cp <sub>2</sub> M <sup>+</sup> ] <sup>c</sup><br>mM | [Cp <sub>2</sub> M] <sup>d</sup><br>mM | W <sub>DP</sub> <sup>e</sup><br>Hz | W <sub>P</sub> <sup>f</sup><br>Hz | δ <sub>DP</sub> <sup>g</sup><br>ppm | δ <sub>D</sub> <sup>h</sup><br>ppm | δ <sub>P</sub> <sup>i</sup><br>ppm | 10 <sup>-7</sup> k <sub>ex</sub> <sup>j</sup><br>M <sup>-1</sup> s <sup>-1</sup> |
|--|--|--|------------------------------------|-----------------------------------|-------------------------------------|------------------------------------|------------------------------------|--|
| HMFC <sup>+/o</sup> Self Exchange at 200.0 MHz and 25°C <sup>k</sup>               |  |  |                                    |                                   |                                     |                                    |                                    |  |
| Acetonitrile <sup>b</sup>  | 1.4  | 36.6                                   | 63                                 | 287                               | 3.41                                | 4.30                               | -20.18                             | 0.54   |
| Propionitrile  | 13.5   | 34.6                                   | 232                                | 319                               | -2.78                               | 4.27                               | -20.85                             | 0.94   |
| Acetone <sup>b</sup>   | 1.1  | 33.8                                   | 45.7                               | 317                               | 3.59                                | 4.33                               | -20.27                             | 0.72   |
| D <sub>2</sub> O   | 4.5  | 5.4                                    | 751                                | 394                               | -7.29                               | 4.33                               | -21.33                             | 1.45   |
| Nitromethane   | 11.35  | 31.2                                   | 179                                | 260                               | -2.34                               | 4.47                               | -21.04                             | 1.4  |
| Benzonitrile   | 5.1  | 33.7                                   | 102                                | 403                               | 1.39                                | 4.54                               | -20.05                             | 1.8  |
| Nitrobenzene <sup>b</sup>  | 0.95   | 26.1                                   | 44.3                               | 450                               | 3.68                                | 4.54                               | -20.47                             | 1.4  |
| Methanol <sup>b</sup>  | 7.5  | 27.4                                   | 177                                | 360                               | -1.30                               | 4.35                               | -21.21                             | 1.7  |
| Cp <sub>2</sub> Co <sup>+/o</sup> Self Exchange at 469.5 MHz and 25°C <sup>b</sup> |  |  |                                    |                                   |                                     |                                    |                                    |  |
| Acetonitrile <sup>b</sup>  | 23.9   | 14.2                                   | 27                                 | 38                                | 8.30                                | 3.91                               | 15.81                              | 19   |
| Acetone <sup>b</sup>   | 22.6   | 10.6                                   | 31                                 | 32                                | 7.49                                | 3.83                               | 15.23                              | 12   |
| D <sub>2</sub> O   | 23.1   | 0.5                                    | 3.5                                | 45                                | 4.17                                | 3.88                               | 16.80                              | ≈30  |
| Nitromethane   | 17.3   | 12.4                                   | 32                                 | 44                                | 8.89                                | 3.93                               | 15.80                              | 24   |
| Benzonitrile   | 18.3   | 2.1                                    | 24                                 | 40                                | 5.15                                | 3.95                               | 15.71                              | 9  |
| Nitrobenzene <sup>b</sup>  | 32   | 0.75                                   | 2.6                                | 51                                | 4.28                                | 4.01                               | 15.76                              | ~4.5   |
| TMU  | 19.6   | 10.0                                   | 79                                 | 63                                | 7.83                                | 3.95                               | 15.47                              | 4.9  |
| PC   | 17.2   | 15.8                                   | 33                                 | 60                                | 9.64                                | 3.93                               | 15.84                              | 14   |
| Methanol <sup>b</sup>  | 27.1   | 11.5                                   | 37                                 | 54                                | 7.78                                | 3.96                               | 16.82                              | 12   |

[See next page for footnotes]

### Footnotes

<sup>a</sup> TMU = tetramethylurea, PC = propylene carbonate.

<sup>b</sup> Deuterated solvent used.

<sup>c</sup> Concentration of oxidized form of redox couple.

<sup>d</sup> Concentration of reduced form of redox couple.

<sup>e</sup> Linewidth (at half height) for diamagnetic-paramagnetic mixture.

<sup>f</sup> Linewidth for pure paramagnetic species (linewidth for pure diamagnetic species taken, or measured to be, 1 Hz in most cases).

<sup>g</sup> Chemical shift (ppm vs. TMS) for diamagnetic-paramagnetic mixture.

<sup>h</sup> Chemical shift for pure diamagnetic species.

<sup>i</sup> Chemical shift for pure paramagnetic species.

<sup>j</sup> Rate constant for self exchange, obtained from listed NMR parameters as outlined in refs. 5a and b.

<sup>k</sup> HMFc = hydroxymethylferrocene; NMR parameters listed refer to methylene proton resonances (see Experimental Section).

<sup>l</sup> Cp\*Co = carboxymethylcobaltocene; NMR parameters listed refer to methyl proton resonances (see Experimental Section).